

# On the Fokas method for the solution of elliptic problems in both convex and non-convex polygonal domains



Matthew J. Colbrook<sup>a,\*</sup>, Natasha Flyer<sup>b</sup>, Bengt Fornberg<sup>c</sup>

<sup>a</sup> Department of Applied Mathematics and Theoretical Physics, University of Cambridge, Cambridge CB3 0WA, UK

<sup>b</sup> Analytics and Integrated Machine Learning, National Center for Atmospheric Research, Boulder, CO 80305, USA

<sup>c</sup> University of Colorado, Department of Applied Mathematics, 526 UCB, Boulder, CO 80309, USA

## ARTICLE INFO

### Article history:

Received 3 January 2018

Received in revised form 31 July 2018

Accepted 1 August 2018

Available online 6 August 2018

### Keywords:

Fokas method/uniform transform method

Elliptic PDEs

Boundary value problems

Corner singularities

## ABSTRACT

There exists a growing literature on using the Fokas method (unified transform method) to solve Laplace and Helmholtz problems on convex polygonal domains. We show here that the convexity requirement can be eliminated by the use of a 'virtual side' concept, thereby significantly increasing the flexibility and utility of the approach. We also show that the inclusion of singular functions in the basis to treat corner singularities can greatly increase the rate of convergence of the method. The method also compares well with other standard methods used to cope with corner singularities. An example is given where this inclusion leads to exponential convergence. As well as this, we give new results on several additional issues, including the choice of collocation points and calculation of solutions throughout domain interiors. An appendix illustrates the algebraic simplicity of the methodology by showing how the core part of the present approach can be implemented in only about a dozen lines of MATLAB code.

© 2018 Elsevier Inc. All rights reserved.

## 1. Introduction

### 1.1. Background to the Fokas method

For many years, the most important open problem associated with non-linear integrable evolution equations was the solution of initial boundary as opposed to initial value problems. A novel approach for the analysis of this problem was introduced by Fokas in [1] and the linear limit of this approach gave rise to a completely new method for solving linear evolution PDEs [2]. Later, it was realised that this method yields new integral representations for the solution of boundary value problems (BVPs) for linear elliptic PDEs in polygonal domains, which in the case of simple domains, can be used to obtain the analytical solution of several problems which apparently cannot be solved by the standard methods [3,4]. The method gives rise to algebraic relations linking the (generalised) Fourier transform of the known boundary data and of the unknown boundary values, which has become known as the *global relation*. Although the global relation is only one of the ingredients of the Fokas method, still this relation has had important analytical and numerical implications: first, it has led to novel analytical formulations of a variety of important physical problems from water waves [5–7] to three-dimensional layer scattering [8]. Second, it has led to the development of new numerical techniques for the Laplace, modified Helmholtz, Helmholtz and biharmonic equations on convex domains. In this paper we shall extend the implementation of this method

\* Corresponding author.

E-mail address: mjc249@cam.ac.uk (M.J. Colbrook).

to solve BVPs on non-convex polygons and introduce basis functions that capture the corner singularities of solutions of generic elliptic BVPs in order to increase the rate of convergence.

Given a *bounded* polygon  $\Omega$  with sides  $\Gamma_j$  listed in positive orientation (anticlockwise), our aim is to numerically solve the elliptic BVP

$$\begin{aligned} u_{xx} + u_{yy} \pm k^2 u &= f \quad \text{in } \Omega, \\ \delta_j u_j^{\mathcal{N}} + A_j u_j &= g_j \quad \text{on } \Gamma_j, \quad j = 1, \dots, n, \end{aligned} \tag{1.1}$$

where  $u_j^{\mathcal{N}}$  denotes the (outward) normal derivative along side  $\Gamma_j$  and  $g_j, f$  are given data. For any side  $\Gamma_j$  we consider two cases: either a Dirichlet boundary condition  $j \in D$  with  $\delta_j = 0$  and  $A_j = 1$ , or a Robin boundary condition  $j \in R$  with  $\delta_j = 1$  and  $A_j$  is a (real) constant. We will deal exclusively with real data  $g_j$  and real solutions  $u$ , but remark that the method can handle complex solutions. We take  $k \in \mathbb{R}_{\geq 0}$  with  $k = 0$  corresponding to the Laplace/Poisson equation,  $+k^2$  the Helmholtz equation and  $-k^2$  the modified Helmholtz equation. The generalised ‘Dirichlet-to-Neumann’ (D2N) problem consists in computing the complementary boundary values, which we denote by  $w_j$ . If  $j \in D$  then this is simply  $w_j = u_j^{\mathcal{N}}$ , otherwise we set  $w_j = A_j u_j^{\mathcal{N}} - u_j$ . The values  $g_j$  and  $w_j$  then determine completely the Dirichlet and Neumann boundary values from which the solution can be reconstructed.

For example, consider the case of the two-dimensional Laplace equation in the variable  $u(x, y)$  formulated in the interior of a closed polygon characterised by the corners  $z_j = x_j + iy_j$ ,  $z_j \in \mathbb{C}$ ,  $j = 1, \dots, n$ . Define  $\hat{u}_j(\lambda)$  as the following Fourier transform along the side  $(z_j, z_{j+1})$ :

$$\hat{u}_j(\lambda) = \int_{z_j}^{z_{j+1}} e^{-i\lambda z} (u_j^{\mathcal{N}} ds + \lambda u_j dz), \quad j = 1, \dots, n, \quad \lambda \in \mathbb{C}, \tag{1.2}$$

with  $s$  denoting the arc length parameterising this side. The global relation in this case is given by

$$\sum_{j=1}^n \hat{u}_j(\lambda) = 0, \quad \lambda \in \mathbb{C}, \tag{1.3}$$

and links the Dirichlet and Neumann boundary values. More generally, the global relation is a key algebraic equation coupling the finite Fourier transforms of the known boundary data  $g_j$  and the unknown boundary values  $w_j$ . In some cases the analysis of the global relation implies that the unknown transforms can be computed through the solution of a Riemann–Hilbert problem [9] and for particular boundary conditions and simple domains this can be bypassed with the unknown transforms computed using only algebraic manipulations. A simple example is the equilateral triangle for which several results generalising the classical results of Lamé can be obtained [10,11].

As mentioned, there has been considerable interest in using the global relations of the Fokas method to evaluate numerically the generalised D2N map [12–27]. The approach consists of two steps. First, one expands the unknown boundary values in some suitable basis. Second, one evaluates the global relations to set up a finite linear system of equations. Assuming the existence of a unique solution to the generalised D2N map, this can be inverted for an approximation of the unknown boundary values given the known boundary data. This method is a *spectral space collocation method* since it involves evaluating a set of equations at different values  $\lambda$  in the complex Fourier plane.<sup>1</sup> It is found that over-determining the system yields smaller condition numbers and we shall take advantage of recent developments in this area [18,25]. This method has recently been put on a more rigorous footing by Ashton [21,28].

### 1.2. Present novelties

Despite its success, the Fokas method has so far been implemented only in *convex* polygons (for numerical reasons we give below) and has mainly been tested on *smooth solutions*, where it yields exponential convergence. These drawbacks are serious when accessing the ability of the Fokas method to solve generic BVPs. This paper addresses these issues and extends the Fokas method in two ways. First, we shall show that a simple decomposition of the domain allows one to deal with *non-convex* polygons in the numerical implementation of the method. In Section 3, we give a heuristic motivation for the convexity requirement for numerical implementations so far presented in the literature. Rigorous results for the Fokas method have only been proven in convex domains, but this is an artificial limitation given the decomposition [21]. A principle of Ehrenpreis [29, Chapter 7] has been described in [24,30,31]: “any solution to a constant coefficient PDE on a convex domain can be written as the superposition of exponential solutions.” This result may also have discouraged explorations with non-convex domains and we stress that the integral representations of the Fokas method do not require

<sup>1</sup> Often when solving PDEs, collocation refers to evaluating at the boundary (e.g. boundary integral methods) and in some cases the interior of the domain. This is not to be confused with collocation in this paper which occurs in spectral, rather than physical, space.

convexity [3], though the integral representation is slightly different in the non-convex case. In particular, the degradation in accuracy when a domain ceases to be convex is not an inevitable consequence of the ‘global relation’ formulation, but instead of a mathematical ‘simplification’, leading to the essence of the proposed novel implementation of the Fokas method. Our implementation does not simplify the resulting matrix and yields a well conditioned numerical method.

Second, we shall present analysis of the inclusion of *singular functions* in the basis, corresponding to *corner singularities*. We demonstrate that the inclusion of singular functions dramatically increases the rate of convergence of the Fokas method for non-smooth solutions. In particular, it is found that the computed unknown boundary values converge at the same rate as their expansion in the chosen basis. This considerably extends the example in [19] that includes one singular function for one corner in the case of Laplace’s equation which is the only example so far in the literature on the Fokas method. For example, we demonstrate that if the solution can be written as an expansion around a singular point in the entire domain, then the Fokas method yields exponential convergence. Scenarios with multiple singular points are also considered, where high-order algebraic convergence is obtained.

There are of course many other methods which seek to solve the BVP in (1.1) such as finite element (FEM), finite difference (FDM), boundary element (BEM), spectral methods etc. Methods designed to cope with corner singularities are extensively reviewed in [32] with strategies such as mesh-refinement [33–35] and schemes which take into account the exact form of the singularities if they are known (an approach which we adopt here). Well known examples include the *hp*-version of the finite element method [36–38], boundary integral methods [39,40], multigrid finite element methods [41] and collocation methods (such as Trefftz methods and radial basis methods) [42,43]. A review of these methods including comparisons with the Fokas method is beyond the scope of this paper, and we limit ourselves to an example in Section 4.3.1 which demonstrates the Fokas method compares well against the singular function boundary integral method, *hp*-FEM and a boundary element formulation treating the corner singularities. For a comparison between the Fokas method and a spectral implementation of the boundary integral method we refer the reader to [19,27]. Rather, our aim is to demonstrate how the limitations of convex domains and smooth solutions can be overcome in the implementation of the Fokas method and we leave to future study further comparisons. Some advantages of the Fokas method studied in this paper include:

- (a) In a similar fashion to boundary integral methods, the Fokas method reduces the dimension of the problem by one and hence the computational cost is much lower than methods which discretise the entire domain (such as FEM and FDM). In addition, all the relevant integrals can be given in closed form and efficiently evaluated in standard environments such as MATLAB. This is in contrast to standard boundary integral formulations which involve the integration of singular functions.
- (b) It is easy to implement. This is illustrated by two short MATLAB codes in the appendix and further example code at the first author’s website: <http://www.damtp.cam.ac.uk/user/mjc249/code.html>. After we have increased the convergence rate through the use of singular functions, this makes it an attractive alternative to *hp*-FEM and other adaptive versions of FEM or BEM which can be difficult to implement. It is also simpler to implement than most collocation methods.
- (c) It is fast, taking typically at most the order of a few seconds on a standard desktop computer (and this can be extended in an efficient manner to evaluate in the domain interior [27]). It shares the efficiency of many collocation methods in that a single (small) linear system is inverted for the solution, with no mesh or discretisation of the domain required.
- (d) The convergence rate is determined by the convergence rate of the expansion of the unknown boundary values,  $w_j$ , in the given basis. For smooth solutions we use a Legendre basis and recover exponential convergence. Once singular functions have been incorporated into the basis, high-order algebraic convergence (and even exponential in some cases) can be achieved for singular solutions.
- (e) In contrast to many collocation methods which typically collocate along the boundary of the domain (or in some cases the domain’s interior), there is a larger degree of freedom in the collocation points (typically  $\mathbb{C} \setminus \{0\}$ ) for the Fokas method. This can be exploited for well-conditioned linear systems [25] and allows for over-determined systems without the clustering of collocation points.<sup>2</sup>

### 1.3. Paper structure

In Section 2 we discuss the problem in more detail and the type of solutions we consider. We also introduce the Fokas method and describe in detail its numerical implementation. Section 3 discusses the implementation in non-convex polygons, including an explanation for ill-conditioning and the idea of virtual sides. We then give numerical examples for the Laplace, modified Helmholtz and Helmholtz equations, finishing with a motivating example for the inclusion of singular functions. Section 4 discusses how to adapt the method to cope with corner singularities and includes numerical examples for the Laplace, modified Helmholtz and Helmholtz equations. Section 5 concludes the paper and discusses future work.

<sup>2</sup> This point has been discussed extensively in [27] in a comparison with the boundary integral method.

## 2. The Fokas method

### 2.1. Conventions and solution type

Before we recall the Fokas method, we will briefly discuss some conventions and the type of solution we are seeking. We list the corners of the polygon in anticlockwise order  $z_1, \dots, z_n$  such that  $\Gamma_j$  joins  $z_j$  to  $z_{j+1}$  with the convention that  $z_{n+1} = z_1$  and each corner  $z_j$  has an internal angle  $\alpha_j \in (0, 2\pi)$ . Since our domain is not smooth, we cannot expect smooth solutions in general. It is well known that if a polygon (or domain with conical points in two dimensions)  $\Omega$  has an angle  $\alpha\pi$  between Neumann and Dirichlet edges corresponding to  $\theta = 0$  and  $\theta = \alpha\pi$  respectively, then for  $1/(2\alpha) \notin \mathbb{Z}$  the leading order singularity for the solution of Laplace's behaves like

$$u \sim r^{1/(2\alpha)} \cos(\theta/(2\alpha)) \tag{2.1}$$

near the corner. Taking  $\alpha \uparrow 1$  we see that even for convex polygons, mixed boundary conditions do not necessarily imply that solutions in  $H^{1+\epsilon}(\Omega)$  for smooth data (this can be made precise and proven with cut-off functions). We refer the reader to [44–47] for some general results on Lipschitz domains.

Let  $\Gamma_D$  be the union of the edges on which we prescribe Dirichlet boundary conditions, along with the corner points between any two adjacent such sides. Similarly define  $\Gamma_R$  for Robin boundary conditions. The following is well known (see for example [48]) and states the well-posedness of our problem if  $f$  and  $g_i$  are sufficiently smooth:

**Theorem 2.1.** *Suppose that  $f \in H^1(\Omega)^*$  (the dual of  $H^1(\Omega)$ ),  $g_D \in H^{1/2}(\Gamma_D)$  and  $g_R \in H^{-1/2}(\Gamma_R)$ . Either there exists a unique  $u \in H^1(\Omega)$  that solves (1.1), or there exists a non-zero solution  $u$  to the corresponding homogeneous problem with  $g_i = 0$ .*

It is precisely for this unique  $H^1(\Omega)$  solution that we numerically compute the generalised D2N map. The points where we have a non-zero solution to the homogeneous problem correspond to when  $\mp k^2$  is an eigenvalue of the Laplacian on  $\Omega$  with homogeneous boundary conditions of the given type. Our numerical experiments will assume that  $\mp k^2$  does not belong to this discrete set.

**Remark 2.2.** It is possible to study the method's global relation (see below) for distributional data [49] and more generally one can study corner asymptotics for maximal domains [50] or distributional boundary data [51,52]. However, we shall stick to the case in Theorem 2.1 for simplicity.

### 2.2. Integral formulation

We now describe how the Fokas method is usually implemented. The starting point is Green's second identity

$$\int_{\partial\Omega} \left( v \frac{\partial u}{\partial n} - u \frac{\partial v}{\partial n} \right) ds = \int_{\Omega} f v dV, \tag{2.2}$$

where  $v$  is any solution of the formal adjoint equation

$$v_{xx} + v_{yy} \pm k^2 v = 0 \text{ in } \Omega. \tag{2.3}$$

Letting  $z = x + iy$  and  $\bar{z} = x - iy$ , for the Poisson equation we take  $v = \exp(-i\lambda z)$  for  $\lambda \in \mathbb{C}$ . Using the general identity (treating  $z$  and  $\bar{z}$  as independent)

$$\frac{\partial F}{\partial n} ds = -i \frac{\partial F}{\partial z} dz + i \frac{\partial F}{\partial \bar{z}} d\bar{z}, \tag{2.4}$$

this yields the equation

$$\int_{\partial\Omega} \exp(-i\lambda z) \left( \frac{\partial u}{\partial n} + \lambda u \frac{dz}{ds} \right) ds = \int_{\Omega} \exp(-i\lambda z) f dV. \tag{2.5}$$

Similarly for the modified Helmholtz equation, we take  $v = \exp((ik/2)(\bar{z}/\lambda - \lambda z))$  for  $\lambda \in \mathbb{C} \setminus \{0\}$  yielding

$$\int_{\partial\Omega} \exp\left( (ik/2)(\bar{z}/\lambda - \lambda z) \right) \left( \frac{\partial u}{\partial n} + \frac{ku}{2} \left( \lambda \frac{dz}{ds} + \frac{1}{\lambda} \frac{d\bar{z}}{ds} \right) \right) ds = \int_{\Omega} \exp\left( (ik/2)(\bar{z}/\lambda - \lambda z) \right) f dV. \tag{2.6}$$

Finally, for the Helmholtz equation we take  $v = \exp((-ik/2)(\bar{z}/\lambda + \lambda z))$  for  $\lambda \in \mathbb{C} \setminus \{0\}$  yielding

$$\int_{\partial\Omega} \exp\left((-ik/2)(\bar{z}/\lambda + \lambda z)\right) \left(\frac{\partial u}{\partial n} + \frac{ku}{2} \left(\lambda \frac{dz}{ds} - \frac{1}{\lambda} \frac{d\bar{z}}{ds}\right)\right) ds = \int_{\Omega} \exp\left((-ik/2)(\bar{z}/\lambda + \lambda z)\right) f dV. \quad (2.7)$$

These equations are known in each case as the global relation, and in fact are an infinite number of equations depending on the complex parameter  $\lambda$ . This is the key property of the Fokas method and is crucial for the following numerical implementations. If  $u$  is real then we obtain a second global relation via Schwartz conjugation (i.e. via taking the complex conjugate and then replacing  $\bar{\lambda}$  with  $\lambda$ ). A complex formulation with exponential type solutions for  $v$  is used due to a deep connection with Fourier analysis that allows one to prove rigorous results [21,28,53], as well as representation formulae (which require integration in the complex plane). Exponential solutions  $v$  also allow explicit expressions for the integrals on the left-hand sides of (2.5)–(2.7) when we expand  $u$  and its normal derivatives in terms of Legendre polynomials and functions that capture corner singularities.

In the particular case of the Helmholtz equation, there is the following similarity of this method with the null-field method [54]: they are both based on Green's (second) identity with one of the two functions equal to the solution of the BVP, and the other function equal to a family of solutions to the adjoint equation (with no boundary conditions). However, even in this particular case there are significant differences: first, the null-field method is specific to the exterior Helmholtz scattering problem, whereas the Fokas method is applied to interior problems. Second, in the former method one chooses the adjoint solutions to be outgoing wave functions found by separation of variables in polar coordinates, whereas in the latter method one chooses the adjoint functions to be the exponential functions found by separation of variables in Cartesian coordinates. Third, and most importantly, in the null-field method one expands the unknown boundary values  $w_j$  in a 'global basis', i.e. the basis functions used for the expansion are supported on the whole of the boundary; common choices of the basis are either the outgoing wave functions themselves, or their normal derivatives (see Section 7.7.2 of [55]). In contrast, in the Fokas method one expands the unknown boundary values  $w_j$  in a 'local basis', i.e. the basis functions are not supported on the whole of the boundary.<sup>3</sup> Using a local basis gives much more flexibility, for example it allows one to incorporate singularities of the solution into the basis.

For the considered case of a polygon, we can parametrise the side  $\Gamma_j$  joining  $z_j$  to  $z_{j+1}$  by  $z = m_j + th_j$ ,  $t \in [-1, 1]$ , with  $m_j = (z_j + z_{j+1})/2$  the midpoint and  $h_j = (z_{j+1} - z_j)/2$  the relevant direction. It follows that  $ds = |h_j| dt$  and we can express the left-hand sides of (2.5) conveniently as

$$\sum_{j=1}^n \exp(-im_j\lambda) \int_{-1}^1 \exp(-i\lambda h_j t) \left(u_j^N |h_j| + \lambda h_j u_j\right) dt. \quad (2.8)$$

Similar expressions can be written down for (2.6) and (2.7). The aim of the method is to approximately solve the linear system for the unknown functions  $w_j$  using the known functions  $g_j$  by evaluating at certain  $\lambda$ .

### 2.3. Approximate global relation and basis choice

An approximate global relation is obtained by expanding the unknown boundary values  $w_j$  in some suitable basis. Various choices of basis can be found in [13,15,17–20,25]. Assuming that the boundary values lie in  $L^2(\Gamma_j)$ , it appears that the best choice of basis is Legendre polynomials. A Fourier basis gives only quadratic convergence for the evaluation of the D2N map for smooth boundary values. Whereas, for sufficiently smooth unknown boundary data (no corner singularities), the use of Chebyshev or Legendre polynomial expansions gives exponential convergence. The key advantage of Legendre polynomials is that we can explicitly compute in closed form the relevant integral transforms.

First expand the unknown boundary values  $w_j$  and the known boundary values  $g_j$  in the Legendre polynomial basis on each side and truncate to  $N$  terms:

$$w_j(t) \approx \sum_{l=0}^{N-1} a_l^j P_l(t), \quad g_j(t) \approx \sum_{l=0}^{N-1} b_l^j P_l(t), \quad (2.9)$$

where  $P_m$  denotes the  $m$ th Legendre polynomial (normalised so that  $P_m(1) = 1$ ). Assuming the boundary data lies in  $L^2(\partial\Omega)$ , this approximation holds in the  $L^2$  sense and the Fourier transform preserves this. We then let

$$\hat{P}_l(\lambda) = \int_{-1}^1 \exp(-i\lambda t) P_l(t) dt, \quad (2.10)$$

denote the Fourier transform of  $P_l$ . Note that this integral transform can be computed in closed form thanks to the relation

<sup>3</sup> These are not to be confused with the 'test functions' which in this case are the separable wave solutions  $v$  which give (2.5)–(2.7).

$$\int_{-1}^1 \exp(\alpha t) P_l(t) dt = \frac{2^{l+1} \alpha^l l!}{(2l+1)} {}_0F_1\left(l + \frac{3}{2}, \frac{\alpha^2}{4}\right) = \frac{\sqrt{2\pi\alpha}}{\alpha} I_{l+\frac{1}{2}}(\alpha), \tag{2.11}$$

where  $I_\nu$  denotes the modified Bessel function of the first kind of order  $\nu$ . This expression is entire in  $\alpha$  and we have chosen to use  $\sqrt{2\pi\alpha}/\alpha$  instead of  $\sqrt{2\pi}/\alpha$  so that the relevant branch cuts along the negative real axis cancel. Most numerical packages have built in functions that can evaluate this closed form expression quickly and accurately such as MATLAB's `besseli`.

2.4. Collocation points

For the Fokas method, collocation occurs in the complex spectral plane, i.e. we evaluate the global relation at different points  $\lambda$ . Various choices of  $\lambda$  have been proposed in the literature, including Halton nodes [19] or certain rays in the complex plane [25]. Given a side  $j$ , we wish to choose  $\lambda$  such that the terms corresponding to this side dominate the approximate global relation. It was shown in [17] (a similar argument holds for the Helmholtz equation) that for a convex polygon this can be achieved by choosing

$$\lambda h_j = -\ell, \quad \frac{k}{2}[-\bar{h}_j/\lambda + \lambda h_j] = -\ell, \quad \frac{k}{2}[\bar{h}_j/\lambda + \lambda h_j] = -\ell \tag{2.12}$$

for some positive real  $\ell$  for the Poisson, modified Helmholtz and Helmholtz equations respectively. After evaluating the system at this point, and multiplying the resulting system by  $\exp(im_j\lambda)$ ,  $\exp(-ik/2[\bar{m}_j/\lambda - \lambda m_j])$  or  $\exp(ik/2[\bar{m}_j/\lambda + \lambda m_j])$  in each case, we find that the exponential contributions from adjacent sides decay linearly for large  $\ell$  and the contributions from other sides further from side  $j$  to decay exponentially as  $l \rightarrow \infty$ . This argument depends crucially on the convexity of the polygon. We also want our system to have similar condition numbers as we vary  $k$ , hence we choose to evaluate the global relation at the points

$$\lambda = -\frac{2\ell/k + \sqrt{(2\ell/k)^2 + 4|h_j|^2}}{2h_j}, \quad \lambda = -\frac{2\ell/k + \sqrt{(2\ell/k)^2 - 4|h_j|^2}}{2h_j}, \tag{2.13}$$

for the modified Helmholtz and Helmholtz equations respectively (see for example [26]). This is done for each side  $j = 1, \dots, n$  and  $\ell$  on  $M$  evenly spaced points in the interval  $[R_1, R_2]$ . Given these points, we evaluate the second global relation (i.e. the Schwartz conjugate) at the complex conjugates of (2.12) and (2.13). We shall refer to (2.12) and (2.13) as ‘ray’ choices. As well as this choice, we shall sometimes choose Halton nodes in a circle of radius  $R$  about the origin, with the idea that this choice avoids clustering of collocation points. Halton nodes have the advantages of simplicity and being independent of the geometry of the domain but generally result in larger condition numbers and loss of accuracy in the method.

2.5. Numerical implementation in convex case

Choosing  $K$   $\lambda$ -values, and discretising along each side with  $N$  Legendre coefficients, the discrete counterpart to (2.5) and its Schwartz conjugate can for a quadrilateral be written for  $f = 0$  as ( $R, S, D$  and  $N$  stand for ‘Regular’, ‘Schwartz conjugate’, ‘Dirichlet’ and ‘Neumann’ respectively):

$$\begin{bmatrix} RD^{(1)} & RN^{(1)} & RD^{(2)} & RN^{(2)} & RD^{(3)} & RN^{(3)} & RD^{(4)} & RN^{(4)} \\ SD^{(1)} & SN^{(1)} & SD^{(2)} & SN^{(2)} & SD^{(3)} & SN^{(3)} & SD^{(4)} & SN^{(4)} \end{bmatrix} \begin{bmatrix} \mathbf{u}_1 \\ \mathbf{u}_1^N \\ \mathbf{u}_2 \\ \mathbf{u}_2^N \\ \mathbf{u}_3 \\ \mathbf{u}_3^N \\ \mathbf{u}_4 \\ \mathbf{u}_4^N \end{bmatrix} = \begin{bmatrix} 0 \\ \vdots \\ \vdots \\ \vdots \\ \vdots \\ \vdots \\ 0 \end{bmatrix}. \tag{2.14}$$

Here  $\mathbf{u}_i$  and  $\mathbf{u}_i^N$  are column vectors, each containing  $N$  Legendre coefficients (corresponding to degrees  $m = 0, 1, \dots, N-1$ ) of the functions  $u_i(t)$  and  $u_i^N(t)$ ,  $i = 1, 2, 3, 4$ . In the case of collocation points (2.12) and (2.13), the Schwartz conjugate of the global relation is not evaluated at the same points and this corresponds to replacing  $SD^{(i)}$  and  $SN^{(i)}$  by the

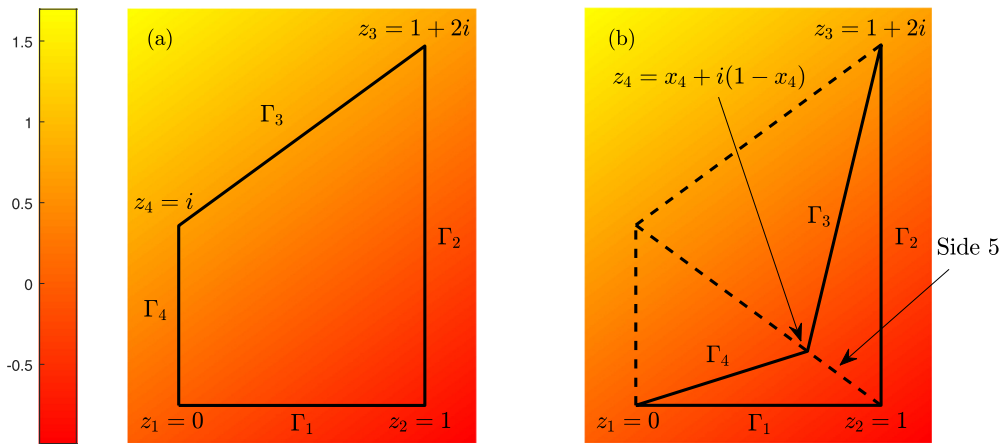


**Fig. 1.** (a) Original quadrilateral in the first test problem, (b) Deformed quadrilateral, with the corner  $z_4$  moving towards the corner  $z_2 = 1$  (which will be used in the non-convex case in Section 3). The colour scale shows the magnitude of a plane wave which, before the non-convex deformation, is dominant on side 3. Oscillations in the plane wave occur along the lines of constant colour shade. No such plane wave exists for points on the boundary near  $z_4$  when we deform as in (b). (For interpretation of the colours in the figure(s), the reader is referred to the web version of this article.)

element-wise complex conjugates of  $RD^{(i)}$  and  $RS^{(i)}$  respectively. For simplicity, we will use the notation  $SD^{(i)}$  and  $SN^{(i)}$  in this case also. Note that each expansion function for the unknowns corresponds to a column of the matrix, whereas the test functions  $v$  used in Green’s identity correspond to two rows (after taking the Schwartz conjugate).

We have graphically displayed the matrix blocks as tall and narrow, to reflect that there typically are many more  $\lambda$ -values than  $m$ -values. The combined matrix (of size  $2K \times 8N$ ) contains in the blocks  $RD^{(i)}$ ,  $RN^{(i)}$ ,  $SD^{(i)}$  and  $SN^{(i)}$  the values for the four integrals in (2.5) and its Schwartz conjugate. For example, listing the collocation points as  $\{\lambda_1, \dots, \lambda_K\}$  and treating the case of Laplace’s equation, we have from (2.8) that

$$\begin{aligned} \{RD^{(j)}\}_{a,b} &= \exp(-im_j\lambda_a)\lambda_a h_j \int_{-1}^1 \exp(-i\lambda_a h_j t) P_{b-1}(t) dt \\ &= \exp(-im_j\lambda_a)\lambda_a h_j \hat{P}(\lambda_a h_j) \quad a = 1, \dots, K, \quad b = 1, \dots, N. \end{aligned} \tag{2.15}$$

Numerical construction of this full matrix is remarkably simple, and requires less than a dozen lines of MATLAB; see the function AB in Appendix A. Given the start and the end point of a side, plus a vector with all the  $K$  different  $\lambda$ -values and the value for  $N$ , this function AB returns the corresponding four matrix blocks  $RD$ ,  $RN$ ,  $SD$  and  $SN$ . This is repeated for each side. Due to variations in the  $\lambda$ -values, the norms can become very different for different rows in (2.14). While scaling of rows does not affect solutions of linear systems with equally many equations as unknowns, it does affect least squares solutions of overdetermined systems. Hence, before proceeding, we normalise to make each row in the coefficient matrix,  $A$ , to have unit  $l^1$  norm  $\sum_{j=1}^{2nN} |A_{i,j}| = 1$ . We then invert in the least squares sense using MATLAB’s backslash command (which in this case uses a QR solver).

For example, consider the case of  $u(x, y) = e^{1+x} \cos(2 + y) = \text{Re}(e^{1+2i+z})$  on the domain shown in Fig. 1 (a). Exact values in this case for all entries in the  $u$ -vector can be obtained by calling the 4-line MATLAB function BV, also given in Appendix A. For standard choices of the parameters, such as  $N = 14$  and  $K = 180$  Halton nodes in a circle of radius  $R = 40$ , multiplying out the matrix-vector product in (2.14) gives a residual less than  $2 \cdot 10^{-14}$ . To solve the D2N problem with, say,  $u_1(t)$ ,  $u_2(t)$ ,  $u_3^N(t)$ ,  $u_4(t)$  given, we first compute the corresponding Legendre coefficient vectors  $\mathbf{u}_1$ ,  $\mathbf{u}_2$ ,  $\mathbf{u}_3^N$ ,  $\mathbf{u}_4$  with the function BV. Inserted into (2.14) and moved to the right hand side, half of the blocks in the matrix (2.14) will be gone, and we are left with a linear system for the remaining vectors  $\mathbf{u}_1^N$ ,  $\mathbf{u}_2^N$ ,  $\mathbf{u}_3$ ,  $\mathbf{u}_4^N$  (overdetermined if  $2K > 4N$ ). With the parameter choices above, these computed solution vectors have a max norm error of about  $2.2 \cdot 10^{-12}$ . The total time for this simple example, averaged over 1000 runs, was  $\approx 0.05$  s on a standard desktop computer. Exactly the same procedure is used for the mixed Dirichlet–Robin boundary conditions in (1.1) where the integral transforms of the known boundary data are moved to the right hand side.

**Remark 2.3.** The method presented here can easily be extended to more general constant coefficient elliptic PDEs. One can either write the PDE in divergence form itself, or after a change of variables, the equation can be transformed into (1.1) except now with Robin boundary conditions replaced by general oblique derivative conditions. This is explored in [11,15,20, 26].

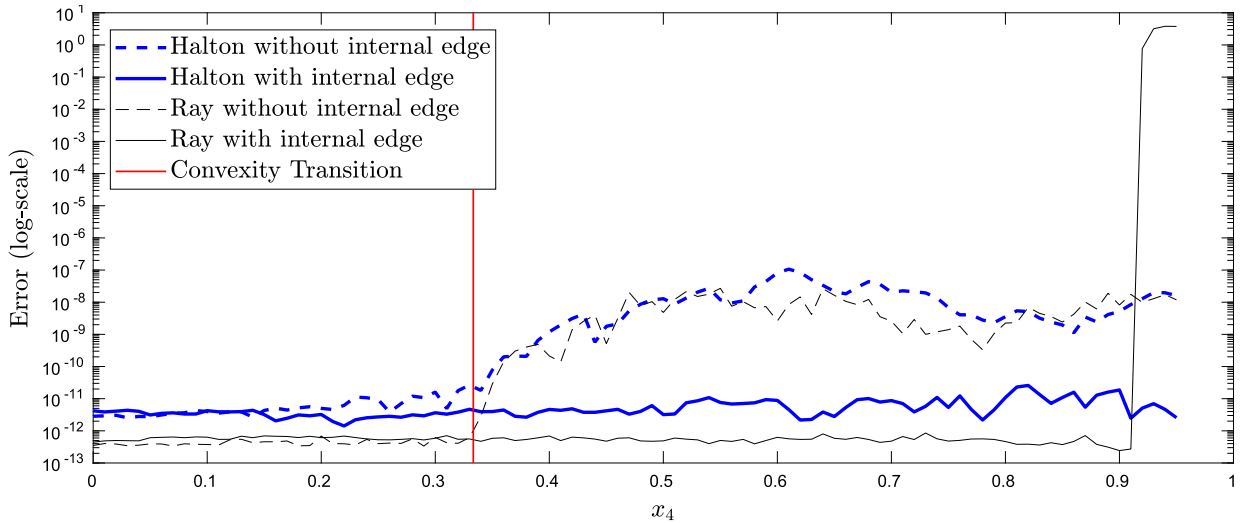


**Fig. 2.** Max error in the Legendre coefficients along all four sides of the quadrilateral, as the corner  $z_4$  is moved towards  $z_2$ . In this case we choose  $K = 180$   $\lambda$ -values and set  $N = 14$ . For the choice corresponding to Halton nodes we set  $R = 50$  and for the choice in (2.12) ('rays' in the complex plane) we set  $R_2 = 30$  and  $R_1 = R_2/M$  following [25]. Parameter dependence is discussed in Section 3.2 but these are near optimal.

### 3. Non-convex polygons

Fig. 1 (b) shows how the quadrilateral in part (a) changes if we gradually move the corner point  $z_4$  from its original position towards  $z_2$ . When  $x_4 = \text{Re}(z_4)$  passes  $1/3$ , the domain ceases to be convex. It is clear from Fig. 2 (dashed curves) that a significant degradation occurs when the domain ceases to be convex. We have shown the maximum error in computed Legendre coefficients for the test problem discussed in Section 2.5 (Laplace).<sup>4</sup> We found similar behaviour for the modified Helmholtz and Helmholtz equations.

A heuristic explanation for this ill-conditioning is as follows: the plane wave 'test functions'  $e^{-i\lambda z}$  in (2.5) (and their counterparts for modified Helmholtz/Helmholtz) grow/decay exponentially in certain directions of  $\lambda$ . When using a sufficiently large selection of complex  $\lambda$ -values, located in all directions from the origin, each side of a convex polygon will for many of these  $\lambda$ -values encounter larger test functions than do the remaining sides, i.e. values along this side will dominate the contributions from the remaining sides. In contrast, for a non-convex polygon, boundaries (and corners) in indented regions will always be dominated by effects from other boundary parts, no matter the  $\lambda$ -value. This is exactly the same argument that motivates the 'ray' choice of collocation points, (2.12), for convex polygons and is shown visually in Fig. 1.

#### 3.1. Proposing a numerically well-conditioned approach – virtual sides

Fig. 1 (b) suggests that the quadrilateral can naturally be split into two triangles by the insertion of a 'side 5' between the corners  $z_4$  and  $z_2$ . Integration of (2.5) around the outer edge of the quadrilateral (sides 1, 2, 3 and 4) could have been done as follows: add the results from following sides 1, 2, and 5 to those from following sides 5 (in reversed direction), 3, and 4. The contributions from side 5 and the values for  $u_5^N$  and  $u_5$  would then cancel. Mathematically, the result becomes identical to just following sides 1, 2, 3 and 4 if we evaluate at the same  $\lambda$ -values.

However, formulas that are mathematically equivalent need not be numerically equivalent. For example, the order in which the equations of a linear system are written down has no influence on the system's solution. Nevertheless, numerical algorithms make extensive use of interchanges (i.e. pivoting) in order to secure numerical stability. This is the situation we encounter here. When integrating along the sides 1, 2, 3 and 4, the numerical conditioning degrades for non-convex domains. In contrast, following the sides of two triangles and then numerically eliminating the results along the shared edge combines two well-conditioned tasks.

The above heuristic argument, together with the following two observations, has provided the impetus for the present study: (i) Boundary integral methods do not encounter any corresponding issues when a domain ceases to be convex, so the issue is not due to the BVP itself nor questions of well-posedness, and (ii) Gaussian elimination with appropriate pivoting is

<sup>4</sup> Note also that for the choice of collocation points (2.12), the error blows up when the polygon becomes degenerate and  $h_5 \rightarrow 0$ . This is not a problem in practice since one bounds the values of  $\lambda$  or replaces  $1/h_j$  by  $\bar{h}_j$ .

well known not to worsen the conditioning of a linear system; thus, letting it handle the merging of well-conditioned tasks ought to be safe. There exists a vast array of methods in the literature that decompose the domain into subdomains and we refer the reader to the introduction [56]. However, no such decomposition has been studied in the context of the Fokas transform.

### 3.2. Numerical implementation of the virtual sides approach

The counterpart to (2.14) will for the two-triangle approach described above takes the form:

$$\begin{bmatrix} RN^{(1)} & 0 & 0 & RN^{(4)} & RD^{(5)} & RN^{(5)} \\ SN^{(1)} & 0 & 0 & SN^{(4)} & SD^{(5)} & SN^{(5)} \\ 0 & RN^{(2)} & RD^{(3)} & 0 & -RD^{(5)} & -RN^{(5)} \\ 0 & SN^{(2)} & SD^{(3)} & 0 & -SD^{(5)} & -SN^{(5)} \end{bmatrix} \begin{bmatrix} \mathbf{u}_1^{\mathcal{N}} \\ \mathbf{u}_2^{\mathcal{N}} \\ \mathbf{u}_3 \\ \mathbf{u}_4^{\mathcal{N}} \\ \mathbf{u}_5 \\ \mathbf{u}_5^{\mathcal{N}} \end{bmatrix} = \begin{bmatrix} RD^{(1)} & 0 & 0 & RD^{(4)} \\ SD^{(1)} & 0 & 0 & SD^{(4)} \\ 0 & RD^{(2)} & RN^{(3)} & 0 \\ 0 & SD^{(2)} & SN^{(3)} & 0 \end{bmatrix} \begin{bmatrix} \mathbf{u}_1 \\ \mathbf{u}_2 \\ \mathbf{u}_3^{\mathcal{N}} \\ \mathbf{u}_4 \end{bmatrix} \quad (3.1)$$

The rightmost blocks in the first matrix in (3.1) (corresponding to side 5 being followed twice, in opposite directions) are identical except with swapped signs. This means we are matching the Cauchy data of the solution in the two subdomains across the virtual side. As just noted, this property makes it tempting to just add the bottom half of all the equations to the top half, eliminating these matrix blocks altogether and, with that, also eliminate the unknowns  $\mathbf{u}_5$ ,  $\mathbf{u}_5^{\mathcal{N}}$  before applying a linear system solver. However, doing this, we get back to the system (2.14), and nothing has been gained. Instead, solving (3.1) as it stands above allows the linear solver to use entirely stable elimination strategies, giving the solid curves in Fig. 2. We no longer see any adverse effect when the quadrilateral loses convexity. The high order coefficients in the vectors  $\mathbf{u}_5$  and  $\mathbf{u}_5^{\mathcal{N}}$  may not end up accurately determined, since side 5 may be very short. However, this does not damage the coefficients along the other sides. Again the method is very quick with typical times  $\approx 0.06$  s, only slightly slower for the larger system.

The accuracy that is reached generally increases with  $N$  (the number of Legendre coefficients used along the sides). Fig. 3 shows the effect, in the present test case, of varying the collocation parameters over wide ranges ( $5 \leq R \leq 100$  and  $20 \leq K \leq 300$ ) for the choice of Halton nodes. In all four cases (original convex quadrilateral vs. worst case when moving the node  $z_4$ , and using original vs. new numerical implementation) large areas emerge with near-constant optimal results, telling that no careful optimisation is needed for these parameters. However they are chosen, the standard implementation is seen to lose about four orders of magnitude in accuracy when the domain loses its convexity. In contrast, the new implementation loses little (if any at all). Fig. 4 shows a similar plot for the ‘ray’ choice of collocation points with exactly the same behaviour. We see that the solution is roughly an order of magnitude more accurate than choosing Halton nodes and the errors are less sensitive to parameter choices.<sup>5</sup>

### 3.3. Test case: L-shaped domain

We now use the idea of virtual sides to solve the Laplace, Helmholtz and modified Helmholtz equations in the domain showed in Fig. 5. As well as computing the unknown boundary values, we shall compute the solution obtained in the interior by the methods in [27]. In each case we prescribe the boundary data  $u + u^{\mathcal{N}}$  (Robin boundary conditions) along sides  $\Gamma_1$  and  $\Gamma_4$ , Neumann data along sides  $\Gamma_2$  and  $\Gamma_5$  and Dirichlet data along sides  $\Gamma_3$  and  $\Gamma_6$ . Analogously to (3.1), this gives rise to the linear system

<sup>5</sup> We did not vary  $R_1$  from  $R_1 = R_2/M$  since we found this parameter to not be as important.

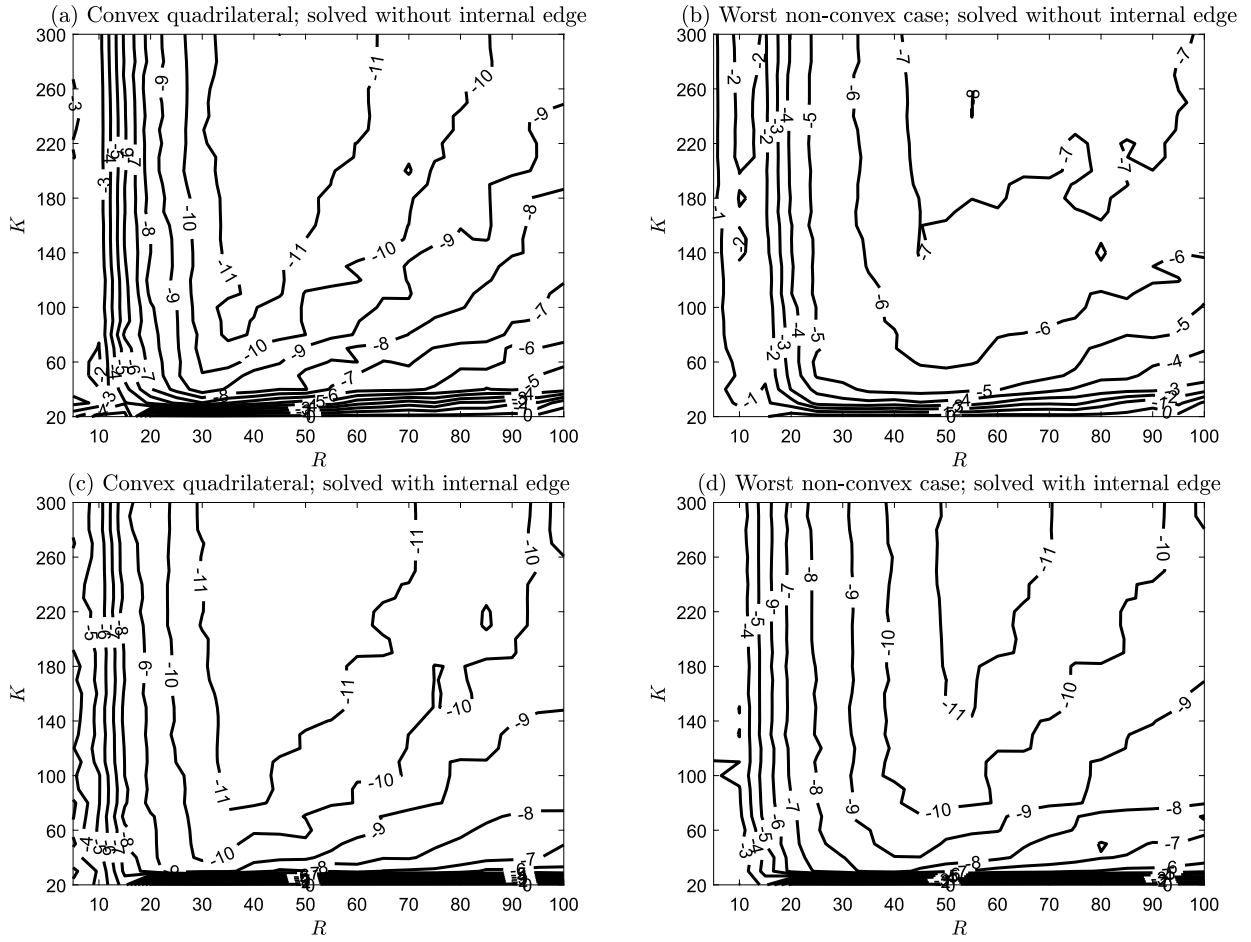


**Fig. 3.** The maximum norm error of computed Legendre coefficients, as functions of the parameters  $K$  and  $R$  in four cases. Top row of subplots: Standard approach with a single quadrilateral: (a) Error for the original quadrilateral shown in Fig. 1 (a), and (b) worst case for any of the deformations shown in Fig. 1 (b) given  $R$  and  $K$  values. Bottom row of subplots: Corresponding results when also including the internal ‘side 5’. All plots are on logarithmic (base 10) scale. We have only considered non-convex polygons up to  $x_4 = 0.7$  to avoid polygons close to being degenerate.

$$\begin{bmatrix} \frac{RN^{(1)}-RD^{(1)}}{2} & RD^{(2)} & RN^{(3)} & 0 & 0 & 0 & RD^{(7)} & RN^{(7)} \\ \frac{SN^{(1)}-SD^{(1)}}{2} & SD^{(2)} & SN^{(3)} & 0 & 0 & 0 & SD^{(7)} & SN^{(7)} \\ 0 & 0 & 0 & \frac{RN^{(4)}-RD^{(4)}}{2} & RD^{(5)} & RN^{(6)} & -RD^{(7)} & -RN^{(7)} \\ 0 & 0 & 0 & \frac{SN^{(4)}-SD^{(4)}}{2} & SD^{(5)} & SN^{(6)} & -SD^{(7)} & -SN^{(7)} \end{bmatrix} \begin{bmatrix} \mathbf{u}_1^{\mathcal{N}} - \mathbf{u}_1 \\ \mathbf{u}_2 \\ \mathbf{u}_3^{\mathcal{N}} \\ \mathbf{u}_1^{\mathcal{N}} - \mathbf{u}_4 \\ \mathbf{u}_5 \\ \mathbf{u}_6^{\mathcal{N}} \\ \mathbf{u}_7 \\ \mathbf{u}_7^{\mathcal{N}} \end{bmatrix} = - \begin{bmatrix} \frac{RN^{(1)}+RD^{(1)}}{2} & RN^{(2)} & RD^{(3)} & 0 & 0 & 0 \\ \frac{SN^{(1)}+SD^{(1)}}{2} & SN^{(2)} & SD^{(3)} & 0 & 0 & 0 \\ 0 & 0 & 0 & \frac{RN^{(4)}+RD^{(4)}}{2} & RN^{(5)} & RD^{(6)} \\ 0 & 0 & 0 & \frac{SN^{(4)}+SD^{(4)}}{2} & SN^{(5)} & SD^{(6)} \end{bmatrix} \begin{bmatrix} \mathbf{u}_1^{\mathcal{N}} + \mathbf{u}_1 \\ \mathbf{u}_2^{\mathcal{N}} \\ \mathbf{u}_3 \\ \mathbf{u}_4^{\mathcal{N}} + \mathbf{u}_1 \\ \mathbf{u}_5^{\mathcal{N}} \\ \mathbf{u}_6 \end{bmatrix} .$$

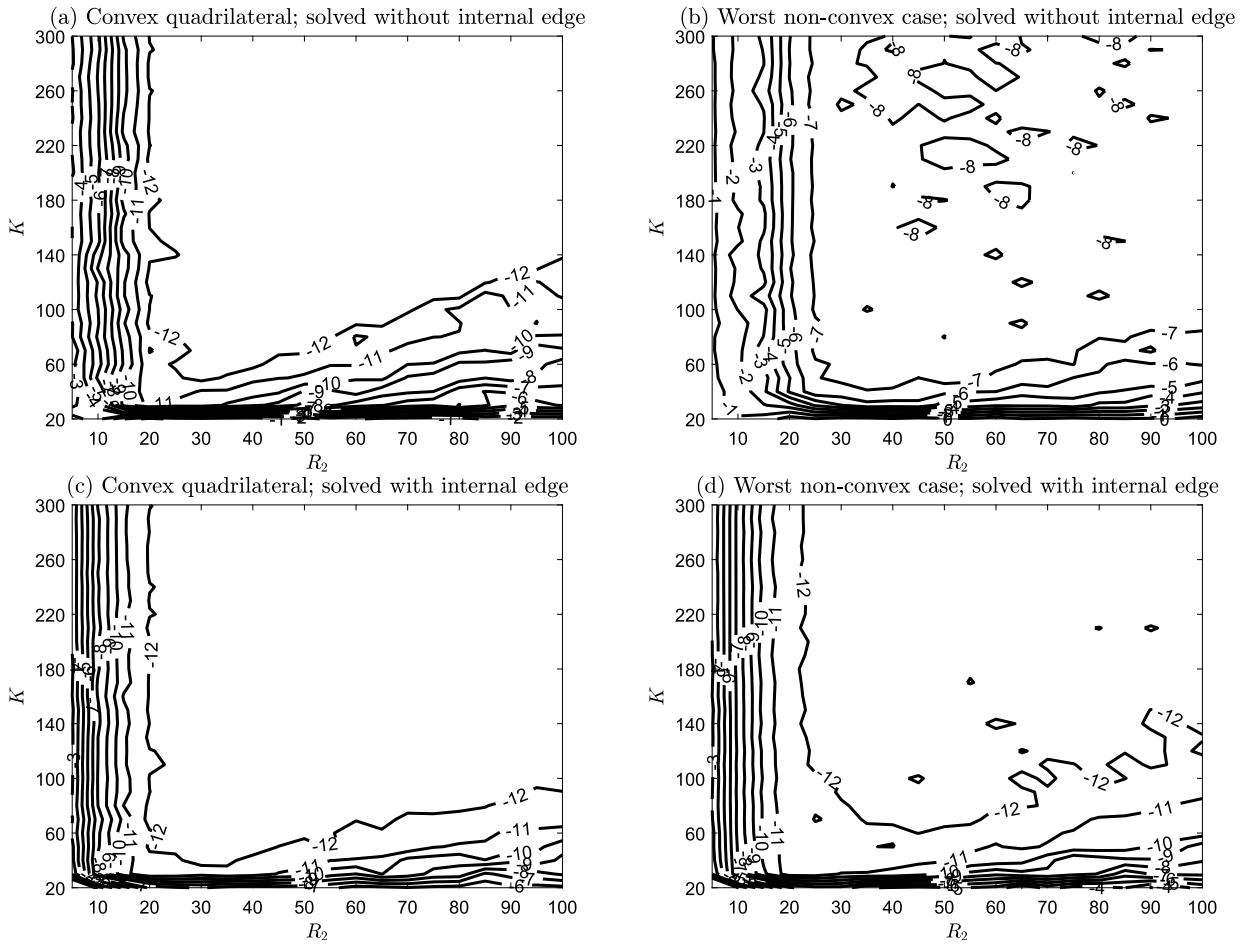


Fig. 4. Same as Fig. 3 but now for the ‘ray’ choice of collocation points.

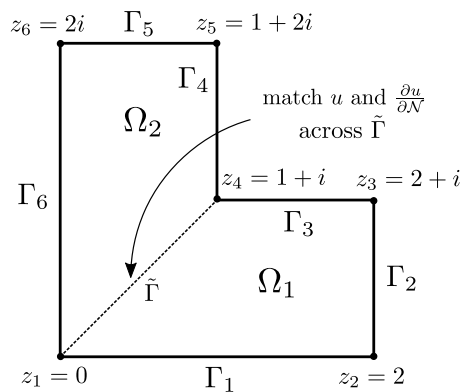


Fig. 5. The geometry of the L-shaped domain and the idea of introducing a virtual side. The domain is split into two convex subdomains  $\Omega_1$  and  $\Omega_2$ .

The form of the approximate solution in the interior of a polygon (given the approximated Dirichlet and Neumann boundary values) was found in [27]. It was shown that it is possible to compute the integrals very efficiently and accurately using a Chebyshev interpolation together with a fast conversion from Chebyshev to Legendre coefficients.

We consider the solutions

$$u(x, y) = \text{Re}(\exp(z) - z^2), \quad u(x, y) = \exp\left(\frac{k}{\sqrt{2}}(x + y)\right), \quad u(x, y) = \text{Re}\left(\exp\left(i\frac{k}{\sqrt{2}}(x + y)\right)\right), \quad (3.2)$$

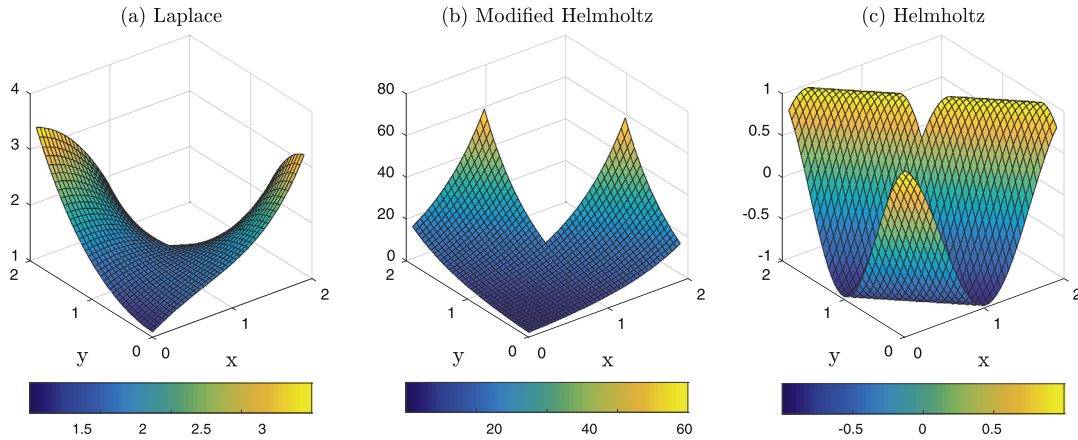


Fig. 6. The analytic solutions for the three test cases considered for the L-shaped domain in Fig. 5.

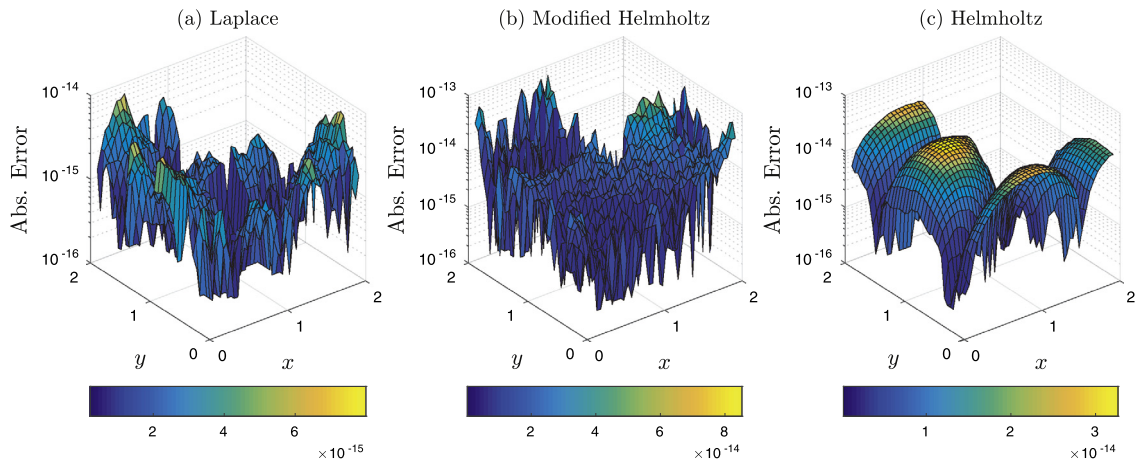


Fig. 7. The absolute errors in the interior for all three test cases at  $N = 20$ .

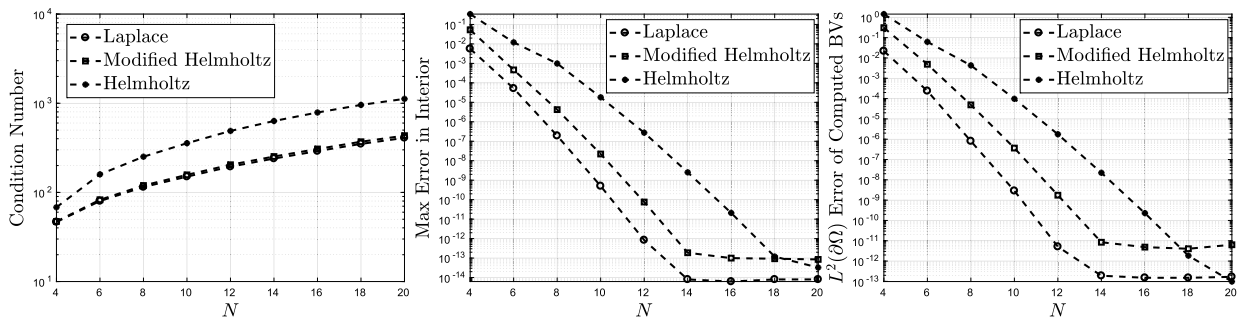


Fig. 8. Left: Condition numbers of the three test cases. Middle: Maximum absolute error over a grid of 1161 points in the interior as a function of  $N$ . The errors decrease exponentially. Right:  $L^2(\partial\Omega)$  error of the computed boundary values as a function of  $N$ . Again, the errors decrease exponentially owing to the smoothness of the solution.

for the Laplace, modified Helmholtz and Helmholtz equations respectively. We choose  $k = 2$  and  $k = 4$  for the modified Helmholtz and Helmholtz equations respectively. Fig. 6 shows the analytic solutions and Fig. 7 shows the absolute errors for the computed solution in the interior for parameters  $R_2 = 10N$ ,  $R_1 = 1/10$  and  $M = 4N$  for the ‘ray’ choice of collocation points in (2.12)–(2.13) at  $N = 20$  over a grid of 1161 points. The computation time for computing the coefficients was  $< 0.1$  s and the solution at the interior points can be computed in a matter of seconds (see [27] for more time results). All errors are bounded by  $10^{-13}$  and the parameters chosen have not been optimised. Fig. 8 shows the maximum error in the

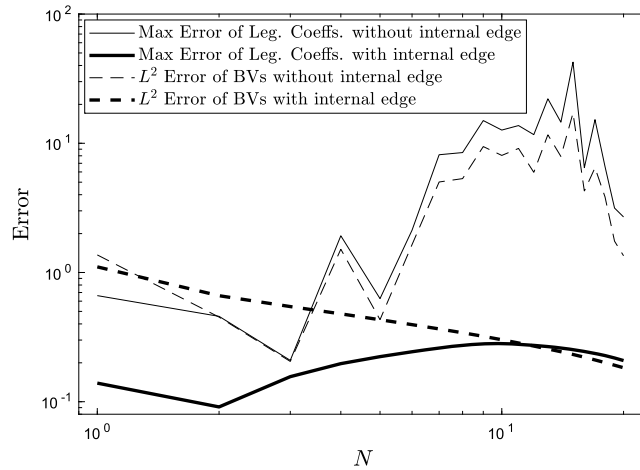


Fig. 9. Max error of the computed Legendre coefficients and the  $L^2(\partial\Omega)$  error of the computed boundary values for the problem in Section 3.4.

interior over these points, the  $L^2(\partial\Omega)$  error of the computed boundary values<sup>6</sup> and the condition numbers as a function of  $N$  for all three test cases. The errors decay exponentially with small condition numbers even for the relatively large choice of  $N = 20$ . In contrast, applying the Fokas method to these problems without the virtual side typically yields errors of at least order  $10^{-6}$  for  $N = 20$ .

### 3.4. Motivating example with corner singularities

As a final motivating example, we shall consider solving Laplace’s equation over the same L-shaped domain but now subject to the boundary conditions  $u_1 = 1$ ,  $u_2^N = 0$ ,  $u_3 = 0$ ,  $u_4 = 0$ ,  $u_5^N = 0$  and  $u_6 = 1$ . We chose  $R_2 = 2N$ ,  $R_1 = 1/10$  and  $M = 8N$  for the ‘ray’ choice of collocation points. Fig. 9 shows the max norm error of the computed Legendre coefficients and the  $L^2(\partial\Omega)$  error of the computed boundary values. These were computed by comparing to the accurate solution obtained in Section 4.3.1. The chosen boundary conditions induce singularities centred at  $z_4$ . Without the internal edge there is no convergence with large sporadic errors. The picture is better with the internal edge but convergence is extremely slow. The  $L^2$  error decreases approximately as  $N^{-1/3}$  consistent with the Legendre expansion of the leading singular function along  $\Gamma_3$  and  $\Gamma_4$  as discussed in Section 4. As we shall see, the problem is in the choice of basis functions and this example motivates the inclusion of singular functions in Section 4. We shall revisit this example in Section 4.3.1 and demonstrate that a proper inclusion of singular functions in the Fokas method can yield exponential convergence.

## 4. Adapting the basis to cope with corner singularities

Previous implementations of the Fokas method have noted algebraic convergence when the boundary data induces corner singularities but exponential convergence for real analytic solutions. This can be explained from the convergence rates of expansions in Legendre polynomials. Suppose we have a function  $F \in L^2((-1, 1))$  that we want to expand in the Legendre basis. It can be shown [57], that if  $F$  can be extended to an analytic function on a neighbourhood of the interval, then convergence is exponentially fast in the  $L^2$  or  $L^\infty$  norm. However, this cannot occur if corner singularities are present in our solution.

An explicit recipe for the construction of singular functions for elliptic systems can be found in [58]. It is well known that the corner singular functions have the asymptotic form

$$\sum_{p \in \mathbb{Z}_{\geq 0}} \sum_{q=0}^{Q(p)} r^{\lambda+p} \log^q r \phi_{p,q}(\theta), \tag{4.1}$$

with  $\phi_{p,q}(\theta)$  analytic, where  $(r, \theta)$  are the local polar coordinates around the corner. Here the exponents  $\lambda$  depend on the angle  $\alpha_j$  as well as the boundary conditions around  $z_j$  and can be derived as eigenvalues of operator pencils [58,59]. The following theorem found in [60] shows why we can only expect algebraic convergence in the presence of such corner singularities.

**Theorem 4.1** (Babuška–Guo [60]). *Let  $F(x) = (x + 1)^\gamma \log^\nu(1 + x)$  on  $(-1, 1)$  where  $\gamma > -1/2$  and  $\nu \in \mathbb{Z}_{\geq 0}$ . Denoting the orthogonal projection onto the first  $N$  Legendre polynomials by  $P_N$ , we have for  $N \geq \max\{1, \gamma\}$  that*

<sup>6</sup> This gives upper bounds on the errors in computed Legendre coefficients.

$$\|F - P_N F\|_2 = N^{-(2\gamma+1)} E_\nu(\gamma, N) \left(1 + \mathcal{O}\left(\frac{1}{N}\right)\right), \tag{4.2}$$

with

$$E_\nu(\gamma, N) = \sum_{k=0}^{\nu} C_{\nu-k}(\gamma) \log^k(1 + N). \tag{4.3}$$

Furthermore, if  $\gamma$  is not an integer then  $C_0 \neq 0$ , if  $\gamma$  is an integer and  $\nu > 0$  then  $C_0 = 0$  but  $C_1 \neq 0$ . Clearly, if  $\gamma$  is an integer and  $\nu = 0$  then there is no approximation error and  $E_\nu(\gamma, N) = 0$ .

However, all is not lost. It turns out that we can separate out the singular parts in the following manner:

**Theorem 4.2** (Kellogg [61]). Suppose we have a  $H^1(\Omega)$  solution of (1.1) and that  $f \in H^s(\Omega)$ ,  $g_j \in H^{s+3/2}(\Gamma_j)$  if  $j \in D$  and  $g_j \in H^{s+1/2}(\Gamma_j)$  if  $j \in R$  for some  $s \geq 0$ . Then there exists a set of exceptional indices  $\mathcal{J}$  such that if  $s \notin \mathcal{J}$  then we can write

$$u = \sum_{k=1}^K c_k v_k + w, \tag{4.4}$$

where:

1.  $w \in H^{s+2}(\Omega)$  and for some  $C > 0$  independent of  $f, g_j$

$$\|w\|_{H^{s+2}(\Omega)} \leq C(\|f\|_{H^s(\Omega)} + \sum_{j \in D} \|g_j\|_{H^{s+3/2}(\Gamma_j)} + \sum_{j \in R} \|g_j\|_{H^{s+1/2}(\Gamma_j)});$$

2. The functions  $v_k$  are the singular functions and are independent of  $f, g_j$ , depend only on the geometry and type of boundary conditions imposed and may be taken to vanish outside a neighbourhood of one of the vertices. They do not lie in  $H^{s+2}(\Omega)$ ;
3. The coefficients  $c_k$  are bounded linear functionals on

$$\{f, g_j\} \in H^s(\Omega) \times \prod_{j \in D} H^{s+3/2}(\Gamma_j) \times \prod_{j \in R} H^{s+1/2}(\Gamma_j);$$

4. The exceptional set  $\mathcal{J}$  does not depend on the data but only on the geometry and type of boundary conditions imposed. It consists of a countable sequence of numbers whose only limit point is  $+\infty$ .

For smooth enough data we can try to subtract off the singular functions from the boundary data using Theorem 4.2 and improve the convergence rate of the basis expansion. We can use the following version of the trace theorem [62] to see that the regular part behaves well on the boundary:

**Theorem 4.3.** Let  $\Omega$  be a bounded open subset of  $\mathbb{R}^2$ , whose boundary is a curvilinear polygon of class  $C^{k,1}$  (i.e. each edge is of class  $C^{k,1}$ ). Then, denoting the trace operator to side  $\Gamma_j$  by  $\gamma_j$ , the mapping

$$u \rightarrow \{\gamma_j u, \gamma_j \frac{\partial u}{\partial n}\}, \quad 1/2 + 1 < s$$

defined for  $u \in \mathcal{D}(\overline{\Omega})$ , has a unique continuous extension as an operator from

$$H^s(\Omega) \text{ onto } H^{s-1/2}(\Gamma_j) \times H^{s-3/2}(\Gamma_j), \quad 2 \leq s \leq k + 1.$$

It was shown in [63] that for any  $s \geq 0$ , there exists a constant  $C$  such that

$$\|F - P_N F\|_2 \leq CN^{-s} \|F\|_{H^s}, \quad \forall F \in H^s((-1, 1)). \tag{4.5}$$

Similar bounds for the uniform norm can be found in [57]. It follows that the boundary data of the regular part of the solution can be well approximated in the basis of Legendre polynomials for large  $s$ .

As mentioned in the introduction, the idea of using these singular functions in numerical solutions of PDEs is not new. Indeed, the singular functions are known to adversely affect the rate of convergence in many methods such as finite element, boundary element, finite difference etc. Refining discretisations/meshes is a standard way to overcome these issues [33–35]. However, it is often more effective to directly include the singular functions in the numerical method [64–69], which is the strategy we adopt here.

#### 4.1. Specific form of the singularities

For convenience, we recall here the well known form of the singular functions for the Poisson, Helmholtz and modified Helmholtz equations with mixed Dirichlet–Neumann boundary conditions. We suppose that we are given boundary conditions on  $\Gamma_1$  and  $\Gamma_2$  with internal angle  $\alpha\pi$  and choose polar coordinates around the corner such that  $\theta = 0$  corresponds to  $\Gamma_2$ . By symmetry, there are three cases to consider and we restrict the exponents so that the solution lies in  $H^1(\Omega)$ , consistent with Theorems 2.1 and 4.2:

**Case 1: We prescribe Dirichlet boundary conditions on sides  $\Gamma_1$  and  $\Gamma_2$ :** In this case we let  $\lambda = l/\alpha$  for  $l \in \mathbb{N}$ . If  $\lambda \notin \mathbb{Z}$  then the singular functions are of the form

- $r^\lambda \sin(\lambda\theta)$  for Laplace;
- $I_\lambda(kr) \sin(\lambda\theta)$  for modified Helmholtz;
- $J_\lambda(kr) \sin(\lambda\theta)$  for Helmholtz;

where  $J_\lambda$  denotes the Bessel function of order  $\lambda$ . If  $\lambda \in \mathbb{Z}$  then the singular functions are of the form  $r^\lambda(\log(r) \sin(\lambda\theta) + \theta \cos(\lambda\theta))$  for the Laplace equation. For the modified Helmholtz and Helmholtz equations the singular function  $v_l$  are of the form

$$I_\lambda(kr)(\log(r) \sin(\lambda\theta) + \theta \cos(\lambda\theta)), \quad J_\lambda(kr)(\log(r) \sin(\lambda\theta) + \theta \cos(\lambda\theta)), \quad (4.6)$$

respectively, up to linear combinations of smooth functions and  $\{v_j\}$  for  $j > l$ . In other words we can use the functions in (4.6) in the expansion (4.4).

**Case 2: We prescribe Dirichlet boundary conditions on side  $\Gamma_1$  but Neumann boundary conditions on  $\Gamma_2$ :** In this case we let  $\lambda = (l - 1/2)/\alpha$  for  $l \in \mathbb{N}$ . If  $\lambda \notin \mathbb{Z}$  then the singular functions are of the form

- $r^\lambda \cos(\lambda\theta)$  for Laplace;
- $I_\lambda(kr) \cos(\lambda\theta)$  for modified Helmholtz;
- $J_\lambda(kr) \cos(\lambda\theta)$  for Helmholtz;

If  $\lambda \in \mathbb{Z}$  then we replace the  $\cos(\lambda\theta)$  by  $(\log(r) \cos(\lambda\theta) - \theta \sin(\lambda\theta))$ .

**Case 3: We prescribe Neumann boundary conditions on sides  $\Gamma_1$  and  $\Gamma_2$ :** In this case we let  $\lambda = l/\alpha$  for  $l \in \mathbb{N}$ . If  $\lambda \notin \mathbb{Z}$  then the singular functions are of the form

- $r^\lambda \cos(\lambda\theta)$  for Laplace;
- $I_\lambda(kr) \cos(\lambda\theta)$  for modified Helmholtz;
- $J_\lambda(kr) \cos(\lambda\theta)$  for Helmholtz;

Again, if  $\lambda \in \mathbb{Z}$  then we replace the  $\cos(\lambda\theta)$  by  $(\log(r) \cos(\lambda\theta) - \theta \sin(\lambda\theta))$ .

**Remark 4.4.** In our numerical examples, we found it sufficient to compute just the first few most singular terms of the asymptotic series and let the Legendre basis approximate the rest.

#### 4.2. Numerical implementation

Our strategy will be to simply supplement our truncated Legendre basis (2.9) along each side with the relevant singular functions which can be computed from the geometry of  $\Omega$  and types of boundary conditions. In order to supplement the basis along the sides adjacent to the corner, we are led (possibly after a change of variables and evaluating the first part of the asymptotic series) to the evaluation of a sum of integrals of the form

$$I(\alpha, m; \rho) = \int_{-1}^1 \exp(\rho t)(1+t)^\alpha \log(1+t)^m dt = \frac{\partial^m}{\partial \alpha^m} \int_{-1}^1 \exp(\rho t)(1+t)^\alpha dt. \quad (4.7)$$

We are only considering the case of corner singularities that lie in  $L^2(\Omega)$ , so we can restrict ourselves to  $\alpha > -1$  which ensures the above integral exists. This integral is analytic as a function of  $\rho$  and the branch-cut of  $(1+t)^\alpha$  is taken to be  $\mathbb{R}_{\leq -1}$  such that the function is real and positive on the positive real axis. A change of variables leads to the integral

$$\frac{\partial^m}{\partial \alpha^m} 2^{\alpha+1} \exp(-\rho) \int_0^1 \exp(2\rho s) s^\alpha ds = \frac{\partial^m}{\partial \alpha^m} \exp(-\rho) \frac{\gamma(\alpha + 1, -2\rho)}{(-\rho)^{\alpha+1}}, \tag{4.8}$$

where  $\gamma(a, z)$  denotes the incomplete gamma function

$$\gamma(a, z) = \int_0^z t^{a-1} \exp(-t) dt \tag{4.9}$$

for  $|\arg(z)| < \pi$  and  $\text{Re}(a) > 0$ , where the path of integration does not cross the negative real axis. Note that the multi-valued nature of  $\gamma$  entirely cancels out that of the power of  $-\rho$ . It is also possible to express  $I(\alpha, m; \rho)$  as a finite linear combination of generalised hypergeometric functions:

$$I(\alpha, m; \rho) = 2^{\alpha+1} \exp(-\rho) \sum_{j=0}^m \binom{m}{j} \log(2)^{m-j} \frac{j!(-1)^j}{(\alpha + 1)^{j+1}} {}_{j+1}F_{j+1}(\alpha + 1, \dots, \alpha + 1; \alpha + 2, \dots, \alpha + 2; 2\rho). \tag{4.10}$$

This can be seen by expanding the exponential in the integral and integrating term by term. For effective numerical evaluation when  $m = 0$ , there exist convenient continued fraction expansions (see [70] equation (8.9.1) and also [71] for effective numerical evaluation). We found that it was sufficient to use MATLAB's `igamma` command for  $m = 0$  and `hypergeom` for  $m > 0$ .

The key difference now is that we have singular functions corresponding to *corners* connecting adjacent sides. For example, suppose we are solving for the Dirichlet values along sides  $\Gamma_{j-1}$  and  $\Gamma_j$  and add a singular function to our basis corresponding to  $\tau_{j-1}(t)$  and  $\tau_j(t)$  along  $\Gamma_{j-1}$  and  $\Gamma_j$  respectively (recall the parametrisation  $t \in [-1, 1]$ ). This adds the column

$$\begin{bmatrix} RD_{\text{sing}}^{(j)} \\ SD_{\text{sing}}^{(j)} \end{bmatrix}$$

to our matrix, where in analogy to (2.15), we have the summed contribution

$$\begin{aligned} \{RD_{\text{sing}}^{(j)}\}_a &= \exp(-im_{j-1}\lambda_a)\lambda_a h_{j-1} \int_{-1}^1 \exp(-i\lambda_a h_{j-1} t) \tau_{j-1}(t) dt \\ &+ \exp(-im_j\lambda_a)\lambda_a h_j \int_{-1}^1 \exp(-i\lambda_a h_j t) \tau_j(t) dt, \end{aligned} \tag{4.11}$$

and  $SD_{\text{sing}}^{(j)}$  its Schwartz conjugate. The extra computed coefficient then corresponds to the singular function. Analogous formulae hold for other types of boundary conditions.

### 4.3. Numerical examples

#### 4.3.1. Laplace

Here we revisit the example considered in Section 3.4. By symmetry the problem can be considered in the trapezoid shown in Fig. 1 (a) with the given boundary conditions  $u_1^N = u_3^N = 0$ ,  $u_2 = 1$  and  $u_4 = 0$ . This is then reflected across  $\Gamma_3$  to obtain the full solution in the L-shaped domain. As mentioned, this problem features one singular point at the corner  $z_4$  with internal angle  $3\pi/4$ . Choosing polar coordinates around  $z_4$  such that  $\theta = 0$  corresponds to  $\Gamma_4$  and defining the functions

$$h_\mu(r, \theta) = r^{2/3(2\mu-1)} \sin\left(\frac{2}{3}(2\mu-1)\theta\right), \quad \mu \in \mathbb{N}, \tag{4.12}$$

it turns out that the solution can be written as

$$u(r, \theta) = \sum_{\mu=1}^{\infty} \alpha_\mu h_\mu.$$

The coefficients  $\alpha_\mu$  are known as (generalised) stress intensity factors which have importance in applications such as elasticity problems with cracks. In many methods such as FEM, these can be computed from the numerical solution [72,73]. We will use the functions  $h_\mu$  as a basis in the entire domain using the integral expressions in Section 4.2 along  $\Gamma_3$  and  $\Gamma_4$ .

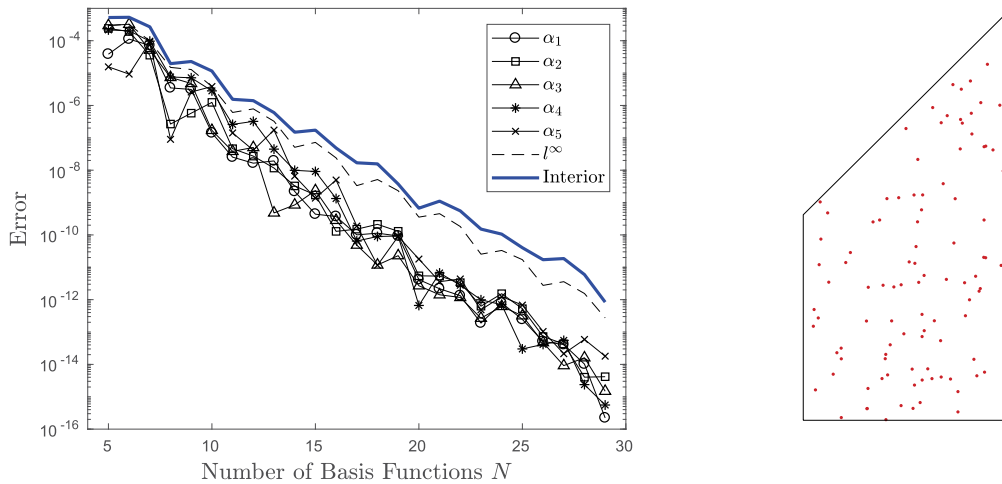


**Fig. 10.** Left: Exponential convergence of the stress intensity factors using the Fokas method and singular functions as a basis. The error over 100 random points in the interior is also shown. Right: Random points at which the error is measured.

**Table 1**

Comparisons of computed  $\alpha_\mu$  with other methods in the literature.

$\mu$	Fokas method		SFBIM [75,76]	<i>hp</i> -FEM [75,76]	BI [77]
1	1.12798040105939	$\pm 0.5 \times 10^{-15}$	1.12798040105939	1.12798010	1.1280
2	0.169933866502253	$\pm 0.5 \times 10^{-16}$	0.16993386650225	0.16993387	0.1699
3	-0.023040973993480	$\pm 0.5 \times 10^{-16}$	-0.02304097399348	-0.0230419	-0.0230
4	0.00347119665822	$\pm 0.5 \times 10^{-15}$	0.0034711966582	0.0034755	0.0035
5	0.00091515709909	$\pm 0.5 \times 10^{-15}$	0.0009151570991	0.0009126	0.0009

Along the sides  $\Gamma_1$  and  $\Gamma_2$ , the  $h_\mu$  contribute smooth parts of the boundary values  $w_j$ . To compute the integral transforms along these sides, we first compute a high order Chebyshev interpolation, convert to Legendre expansions and then use the expression (2.11) in terms of Bessel functions. Fig. 10 shows the exponential convergence of the first 5 coefficients  $\alpha_\mu$  where the error was computed by comparing to converged values computed for larger  $N$ . Similar exponential convergence occurs for the other expansion coefficients and we have shown the  $l^\infty$  error of the whole computed vector of coefficients. We found it was useful to use a mixture of the ‘ray’ choice of collocation points ( $M = 2N$ ,  $R_1 = 1/10$  and  $R_2 = 2N$ ) together with a few Halton nodes ( $4N$  of these in a circle of radius 10). The maximum absolute error of the computed solution over 100 randomly selected points in the interior is also shown in Fig. 10 and agrees well with the  $l^\infty$  error of the whole computed vector of coefficients.

This problem is special in that a global basis can be written down via separation of variables around a singular point. Another method proposed in the literature for such problems is the so called singular function boundary integral method (SFBIM) [74]. This method uses the same expansion but enforces the boundary conditions weakly via Lagrange multipliers. Comparisons of the Fokas method ( $N = 35$  basis functions), SFBIM (values from [75,76] using  $N = 60$  basis functions and 41 Lagrange multipliers), *hp*-FEM (values from [75,76] using the commercial FEM package STRESSCHECK with 691 degrees of freedom, refined mesh near singularity and up to degree eight polynomial elements) and a boundary element formulation treating the corner singularities (values from [77] using 256 linear elements per side with first five singular functions) are shown in Table 1. The Fokas method is able to obtain the most accurate values of the coefficients (and this extends to more coefficients when comparing Fig. 10 to the results of [76]). It also requires fewer basis functions than SFBIM and is much simpler to implement than the other methods. Next we shall see that the Fokas method can also cope with solutions with multiple singular points.

#### 4.3.2. Modified Helmholtz and Helmholtz

In this example we will study the modified Helmholtz equation and Helmholtz equation for  $k = 1/2$  on the same trapezoid shown in Fig. 1 (a). The boundary conditions chosen are  $u_1^N = 0$ ,  $u_2 = 1$ ,  $u_3^N = 0$  and  $u_4(t) = t$ . These induce singular functions at multiple corners of the form studied in Section 4.1. To compare with the convergence rates predicted in Theorem 4.1, we can group the singularities at each corner so that successively including each group increases the convergence rate (up to logarithmic factors) of the Legendre expansion of the remaining ‘smooth’ part. For this example, the expected rates (up to logarithmic factors) are  $1/3$ ,  $1$ ,  $3$ ,  $5$  and so on. Fig. 11 and 12 show the results for the modified Helmholtz and Helmholtz equations respectively. We used the ‘ray’ choice of collocation points with  $M = 5N$ ,  $R_1 = 1/10$  and  $R_2 = 5N$ . We did not have a reference solution to compare against so compared to a ‘converged’ solution computed with larger  $N$ .

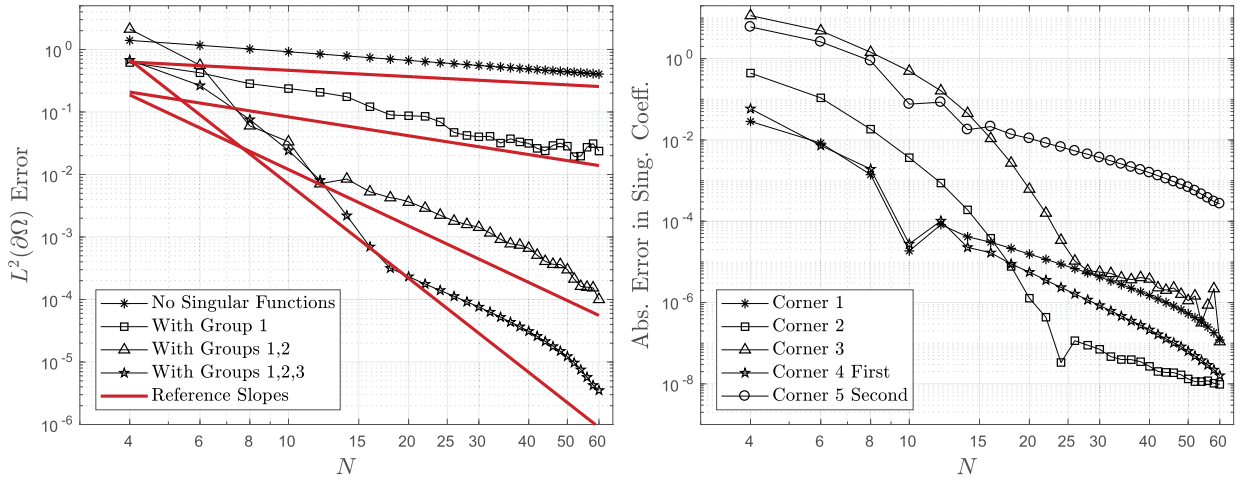


**Fig. 11.** Results for the modified Helmholtz equation. Left:  $L^2(\partial\Omega)$  error in the estimate of the boundary values (non-singular function part) as we include successive groups of singular functions in our basis. The reference slopes are  $-1/3$ ,  $-1$ ,  $-3$  and  $-5$  as predicted by Theorem 4.1. Right: The absolute error in the computed singular function coefficients as we increase  $N$  (when including groups 1, 2 and 3).

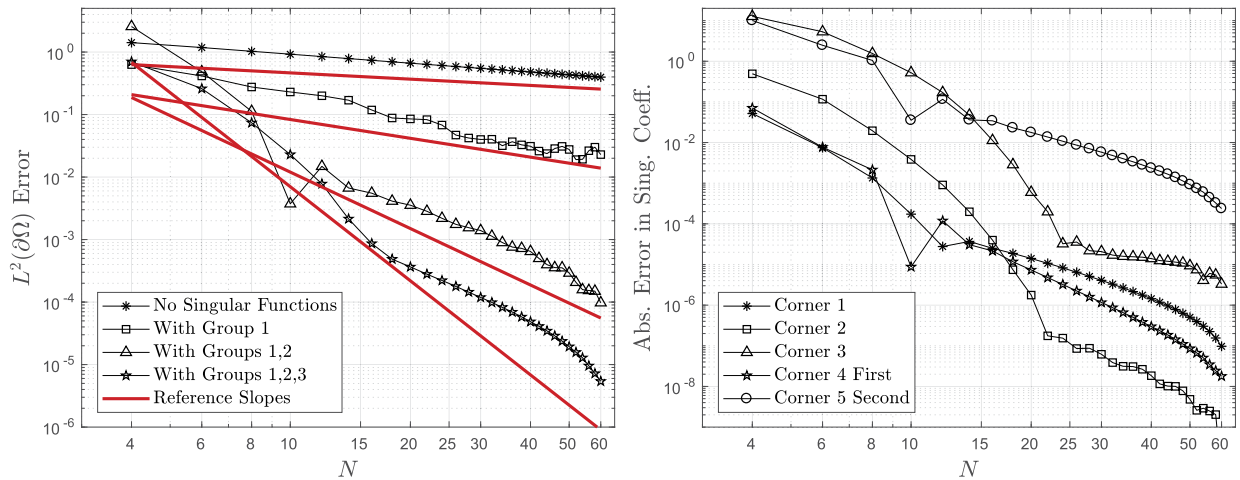


**Fig. 12.** Same as Fig. 11 but for the Helmholtz equation.

The agreement between the rate of convergence of the Legendre expansions from Theorem 4.1 and the computed rates shows strong numerical evidence that the Fokas method converges at the same rate as the expansion basis. We have also shown the convergence of the coefficients of the five singular functions when we include groups 1 to 3. However, as the included singular functions become smoother and better approximated by their Legendre expansion, the condition number of the system increases. For example with  $N = 60$  it increases from  $\approx 10^4$  when no singular functions are included to  $\approx 10^{10}$  when the first five singular functions are included. We found this to be a problem for smoother singular functions than those shown in Figs. 11 and 12 – we did not see a noticeable improvement in the rate of convergence. Similar qualitative results were found when considering this problem for the Helmholtz equation and also for various choices of  $k$ .

### 5. Conclusion

The requirement for domain convexity does not seem to have been seriously questioned so far in the Fokas method literature on elliptic PDEs. We have here provided evidence through heuristic arguments as well as test problems that accuracy losses in non-convex cases are not inevitable consequences of the Fokas method concept, but are entirely avoidable. The problem arises when a key elimination step for the linear system is carried out analytically, without regard to conditioning issues, instead of numerically, in which case standard pivoting strategies within linear solvers will successfully deal with the issue.

As well as this, we have extended the earlier example in the literature and have shown that the inclusion of corner singularities can greatly enhance the solution’s accuracy if it is not smooth. This is important when using the Fokas method

for real-life problems. Our results show that the method typically converges at the same rate of the Legendre expansion of the most singular function not included in the basis. An example with corner singularities was given where the Fokas method produced exponential convergence and compared well against other methods in the literature. One remaining challenge in this area is to find ways to reduce the condition number of the system as more singular functions are included in the basis. This, and consideration of other basis choices (which may lower the condition number), is currently under investigation.

No proofs of convergence of the method have been given, and proving the method converges is likely to be subtle. This is essentially due to the fact that the analysis depends on the values of an analytic function on a compact subset of  $\mathbb{C}$  and it is easy to construct functions  $f_m$  on  $[-1, 1]$  with  $L^2$  norm 1 that have  $\hat{f}_m \rightarrow 0$  locally uniformly in  $\mathbb{C}$ . A proof of convergence is work in progress. Current work is also investigating the exterior problem [78,79] and more general curvilinear polygons with curved edges. For the exterior problem, by evaluating an additional equation obtained as a limit in the interior of the polygon, it should be possible to determine the expansion coefficients of the unknown boundary values. Then, the appropriately modified global relations yield the scattering amplitudes [80].

Finally, we believe that this paper sets the stage for further comparisons between the Fokas method and other more standard methods. Further comparisons are beyond the scope of this paper but we note that for such comparisons it is crucial to consider non-convex domains and non-smooth solutions to assess the Fokas method. The methods provided in this paper are a first step in this direction.

## Acknowledgements

MJC acknowledges support from EPSRC grant EP/L016516/1 for the University of Cambridge Centre for Doctoral Training, the Cambridge Centre for Analysis. The National Center for Atmospheric Research is sponsored by NSF.

## Appendix A. Example of easy-to-use code

The following is a listing of a MATLAB function AB that calculates the blocks of the linear system matrix corresponding to a side extending from a start point  $z_s$  to an end point  $z_e$ :

```
function [RD,RN,SD,SN] = AB(zs,ze,lambda,N)

% Calculate the matrix blocks that correspond to a line segment that
% goes from point zs to point ze

% Input parameters
% zs,ze Start and end points of line segment (complex)
% lambda Column vector (complex), all K different lambda-values
% N Number of Legendre coefficients, i.e. degrees 0, 1, ..., N-1
% Output parameters
% RD Array (K,N); part 'Regular Dirichlet' of system matrix
% RN Array (K,N); part 'Regular Neumann' of system matrix
% SD Array (K,N); part 'Schwartz Dirichlet' of system matrix
% SN Array (K,N); part 'Schwartz Neumann' of system matrix

% Exact integral of exp(alpha*t)*P_m(t), {t,-1,1}
LI = @(m,alpha) sqrt(2*pi*alpha)./alpha.*besseli(m+0.5,alpha);

K = length(lambda);
RD = zeros(K,N); RN = zeros(K,N);SD = zeros(K,N);SN = zeros(K,N);

for m = 0:N-1 % Loop over the degrees of Legendre polynomials
    RI = 0.5*exp(-0.5i*lambda*(zs+ze)) .* LI(m,-0.5i*lambda*(ze-zs));
    RS = 0.5*exp(0.5i*lambda*conj(zs+ze)) .* LI(m,0.5i*lambda*conj(ze-zs));
    RD(:,m+1) = lambda*(ze-zs) .*RI;
    RN(:,m+1) = abs(ze-zs) .*RI;
    SD(:,m+1) = lambda*conj(ze-zs) .*RS;
    SN(:,m+1) = abs(ze-zs) .*RS;
end
```

For test problems with an analytic solution of the form  $u(z) = e^{a+bz}$  (or its real part), the following routine provides values for  $u$  and  $u^N$  along a line segment from  $z_s$  to  $z_e$ :

```

function [LD, LN] = BV(zs, ze, a, b, N)

% Create Legendre coefficients for the Dirichlet and Neumann data for the
% test function f(z) = exp(a+b*z) along the line segment from zs to ze.

% Input parameters
%   zs, ze   Start and end points of line segment (complex)
%   a, b     Parameters defining the test function f(z) = exp(a+b*z)
%   N       Number of Legendre coefficients; use degrees up through N-1
% Output parameters
%   LD, LN   Column vectors with the first N Legendre coefficients for the
%           test function's Dirichlet and Neumann data, respectively

% Exact integral of exp(alpha*t)*P_m(t), {t, -1, 1}
LI = @(m, alpha) sqrt(2*pi*alpha) ./ alpha .* besseli(m+0.5, alpha);

m = (0:N-1)'; % Column vector with the Legendre degrees to be used
LD = (m+0.5)*exp(a+b*zs+0.5*(ze-zs)*b) .* LI(m, 0.5*(ze-zs)*b);
LN = -1i*(ze-zs)*b*LD/abs(zs-ze);

```

For more complicated boundary data, the Legendre expansion coefficients can be computed accurately using quadrature.

## References

- [1] A.S. Fokas, A unified transform method for solving linear and certain nonlinear PDEs, *Proc. R. Soc. A* 453 (1997) 1411–1443.
- [2] Bernard Deconinck, Thomas Trogdon, Vishal Vasan, The method of Fokas for solving linear partial differential equations, *SIAM Rev.* 56 (1) (2014) 159–186.
- [3] E.A. Spence, *Boundary Value Problems for Linear Elliptic PDEs*, PhD thesis, University of Cambridge, 2011.
- [4] K. Kalimeris, *Initial and Boundary Value Problems in Two and Three Dimensions*, PhD thesis, University of Cambridge, 2010.
- [5] B. Deconinck, K. Oliveras, The instability of periodic surface gravity waves, *J. Fluid Mech.* 675 (2011) 141–167.
- [6] K.L. Oliveras, V. Vasan, B. Deconinck, D. Henderson, Recovering the water-wave profile from pressure measurements, *SIAM J. Appl. Math.* 72 (3) (2012) 897–918.
- [7] V. Vasan, B. Deconinck, The inverse water wave problem of bathymetry detection, *J. Fluid Mech.* 714 (2013) 562–590.
- [8] D.M. Ambrose, D.P. Nicholls, Fokas integral equations for three dimensional layered-media scattering, *J. Comput. Phys.* 276 (2014) 1–25.
- [9] A.S. Fokas, A.A. Kapaev, On a transform method for the Laplace equation in a polygon, *IMA J. Appl. Math.* 68 (4) (2003) 355–408.
- [10] G. Dassios, A.S. Fokas, The basic elliptic equations in an equilateral triangle, *Proc. R. Soc., Math. Phys. Eng. Sci.* 461 (2005) 2721–2748.
- [11] A.S. Fokas, K. Kalimeris, Eigenvalues for the Laplace operator in the interior of an equilateral triangle, *Comput. Methods Funct. Theory* 14 (1) (2014) 1–33.
- [12] A.S. Fokas, Two-dimensional linear partial differential equations in a convex polygon, *Proc. R. Soc. A* 457 (2001) 371–393.
- [13] S.R. Fulton, A.S. Fokas, C.A. Xenophontos, An analytical method for linear elliptic PDEs and its numerical implementation, *J. Comput. Appl. Math.* 167 (2) (2004) 465–483.
- [14] A.G. Sifalakis, E.P. Papadopoulou, Y.G. Saridakis, Numerical study of iterative methods for the solution of the Dirichlet–Neumann map for linear elliptic PDEs on regular polygon domains, *Int. J. Appl. Math. Comput. Sci.* 4 (2007) 173–178.
- [15] A.G. Sifalakis, A.S. Fokas, S.R. Fulton, Y.G. Saridakis, The generalized Dirichlet–Neumann map for linear elliptic PDEs and its numerical implementation, *J. Comput. Appl. Math.* 219 (1) (2008) 9–34.
- [16] A.G. Sifalakis, S.R. Fulton, E.P. Papadopoulou, Y.G. Saridakis, Direct and iterative solution of the generalized Dirichlet–Neumann map for elliptic PDEs on square domains, *J. Comput. Appl. Math.* 227 (1) (2009) 171–184.
- [17] A.S. Fokas, N. Flyer, S.A. Smitheman, E.A. Spence, A semi-analytical numerical method for solving evolution and elliptic partial differential equations, *J. Comput. Appl. Math.* 227 (1) (2009) 59–74.
- [18] S.A. Smitheman, E.A. Spence, A.S. Fokas, A spectral collocation method for the Laplace and modified Helmholtz equations in a convex polygon, *IMA J. Numer. Anal.* 30 (4) (2010) 1184–1205.
- [19] B. Fornberg, N. Flyer, A Numerical Implementation of Fokas Boundary Integral Approach: Laplace's Equation on a Polygonal Domain, *Proc. R. Soc. A* 467 (2011) 2983–3003.
- [20] Y.G. Saridakis, A.G. Sifalakis, E.P. Papadopoulou, Efficient numerical solution of the generalized Dirichlet–Neumann map for linear elliptic PDEs in regular polygon domains, *J. Comput. Appl. Math.* 236 (9) (2012) 2515–2528.
- [21] A.C.L. Ashton, The spectral Dirichlet–Neumann map for Laplace's equation in a convex polygon, *SIAM J. Math. Anal.* 45 (6) (2013) 3575–3591.
- [22] A.S. Fokas, A. Iserles, S.A. Smitheman, The unified method in polygonal domains via the explicit Fourier transform of Legendre polynomials, in: *Unified Transforms*, SIAM, Philadelphia, PA, 2014, 2014.
- [23] C.I.R. Davis, B. Fornberg, A spectrally accurate numerical implementation of the Fokas transform method for Helmholtz-type PDEs, *Complex Var. Elliptic Equ.* 59 (4) (2014) 564–577.
- [24] A.C.L. Ashton, Elliptic PDEs with constant coefficients on convex polyhedra via the unified method, *J. Math. Anal. Appl.* 425 (1) (2015) 160–177.
- [25] P. Hashemzadeh, A.S. Fokas, S.A. Smitheman, A numerical technique for linear elliptic partial differential equations in polygonal domains, *Proc. R. Soc. A* 471 (2015).
- [26] M.J. Colbrook, A.S. Fokas, Computing eigenvalues and eigenfunctions of the Laplacian for convex polygons, *Appl. Numer. Math.* 126 (2018) 1–17.
- [27] M.J. Colbrook, A.S. Fokas, P. Hashemzadeh, A hybrid analytical–numerical technique for elliptic PDEs, submitted for publication.
- [28] A.C.L. Ashton, On the rigorous foundations of the Fokas method for linear elliptic partial differential equations, *Proc. R. Soc. A* 468 (2012) 1325–1331.
- [29] L. Ehrenpreis, *Fourier Analysis in Several Complex Variables*, Courier Corporation, 2011.
- [30] A.C.L. Ashton, Laplace's equation on convex polyhedra via the unified method, *Proc. R. Soc. A* 471 (2015) 20140884.
- [31] A.S. Fokas, E.A. Spence, Synthesis, as opposed to separation, of variables, *SIAM Rev.* 54 (2) (2012) 291–324.

- [32] Z.-C. Li, T.-T. Lu, Singularities and treatments of elliptic boundary value problems, *Math. Comput. Model.* 31 (8–9) (2000) 97–145.
- [33] H. Motz, The treatment of singularities of partial differential equations by relaxation methods, *Q. Appl. Math.* 4 (4) (1947) 371–377.
- [34] T. Apel, A.-M. Sändig, J.R. Whiteman, Graded mesh refinement and error estimates for finite element solutions of elliptic boundary value problems in non-smooth domains, *Math. Methods Appl. Sci.* 19 (1) (1996) 63–85.
- [35] T. Apel, S. Nicaise, The finite element method with anisotropic mesh grading for elliptic problems in domains with corners and edges, *Math. Methods Appl. Sci.* 21 (6) (1998) 519–549.
- [36] B. Guo, I. Babuška, The  $hp$  version of the finite element method, *Comput. Mech.* 1 (1) (1986) 21–41.
- [37] I. Babuška, B.Q. Guo, Regularity of the solution of elliptic problems with piecewise analytic data. Part I. Boundary value problems for linear elliptic equation of second order, *SIAM J. Math. Anal.* 19 (1) (1988) 172–203.
- [38] I. Babuška, B.Q. Guo, Regularity of the solution of elliptic problems with piecewise analytic data. Part II: the trace spaces and application to the boundary value problems with nonhomogeneous boundary conditions, *SIAM J. Math. Anal.* 20 (4) (1989) 763–781.
- [39] N.K. Mukhopadhyay, S.K. Maiti, A. Kakodkar, A review of SIF evaluation and modelling of singularities in BEM, *Comput. Mech.* 25 (4) (2000) 358–375.
- [40] G.T. Symm, *Treatment of Singularities in the Solution of Laplace's Equation by an Integral Equation Method*, National Physical Laboratory, Division of Numerical Analysis and Computing, 1973.
- [41] Y. Zhu, A.C. Cangellaris, *Multigrid Finite Element Methods for Electromagnetic Field Modeling*, vol. 28, John Wiley & Sons, 2006.
- [42] B. Fornberg, N. Flyer, *A Primer on Radial Basis Functions with Applications to the Geosciences*, SIAM, 2015.
- [43] Z.-C. Li, T.-T. Lu, H.-Y. Hu, A.H.D. Cheng, Trefftz and Collocation Methods, WIT Press, 2008.
- [44] D.S. Jerison, C.E. Kenig, The Neumann problem on Lipschitz domains, *Bull. Am. Math. Soc.* 4 (2) (1981) 203–207.
- [45] D. Jerison, C.E. Kenig, The inhomogeneous Dirichlet problem in Lipschitz domains, *J. Funct. Anal.* 130 (1) (1995) 161–219.
- [46] C.E. Kenig, *Harmonic Analysis Techniques for Second Order Elliptic Boundary Value Problems*, vol. 83, American Mathematical Soc., 1994.
- [47] G. Savaré, Regularity results for elliptic equations in Lipschitz domains, *J. Funct. Anal.* 152 (1) (1998) 176–201.
- [48] W. Charles, H. McLean, *Strongly Elliptic Systems and Boundary Integral Equations*, Cambridge University Press, 2000.
- [49] A.C.L. Ashton, A.S. Fokas, Elliptic boundary value problems in convex polygons with low regularity boundary data via the unified method, arXiv: 1301.1490, 2013.
- [50] A. Kubica, The regularity of weak and very weak solutions of the Poisson equation on polygonal domains with mixed boundary conditions (part II), *Appl. Math.* 32 (2005) 17–36.
- [51] I. Babuška, V. Nistor, Boundary value problems in spaces of distributions on smooth and polygonal domains, *J. Comput. Appl. Math.* 218 (1) (2008) 137–148.
- [52] A.K. Aziz, R.B. Kellogg, et al., On homeomorphisms for an elliptic equation in domains with corners, *Differ. Integral Equ.* 8 (2) (1995) 333–352.
- [53] A.C.L. Ashton, K.M. Crooks, Numerical analysis of Fokas' unified method for linear elliptic PDEs, *Appl. Numer. Math.* 104 (2016) 120–132.
- [54] R.E. Kleinman, G.F. Roach, S.E.G. Ström, The null field method and modified Green functions, *Proc. R. Soc. Lond. A* 394 (1806) (1984) 121–136.
- [55] P.A. Martin, *Multiple Scattering: Interaction of Time-Harmonic Waves with N Obstacles*, vol. 107, Cambridge University Press, 2006.
- [56] T. Mathew, *Domain Decomposition Methods for the Numerical Solution of Partial Differential Equations*, vol. 61, Springer Science & Business Media, 2008.
- [57] H. Wang, S. Xiang, On the convergence rates of Legendre approximation, *Math. Comput.* 81 (278) (2012) 861–877.
- [58] M. Costabel, M. Dauge, Construction of corner singularities for Agmon–Douglis–Nirenberg elliptic systems, *Math. Nachr.* 162 (1) (1993) 209–237.
- [59] V.A. Kozlov, V.G. Mazia, J. Rossmann, *Spectral Problems Associated with Corner Singularities of Solutions to Elliptic Equations*, vol. 85, American Mathematical Soc., 2001.
- [60] I. Babuška, B. Guo, Optimal estimates for lower and upper bounds of approximation errors in the  $p$ -version of the finite element method in two dimensions, *Numer. Math.* 85 (2) (2000) 219–255.
- [61] R.B. Kellogg, Higher order singularities for interface problems, in: *The Mathematical Foundations of the Finite Element Method with Applications to Partial Differential Equations*, Proc. Sympos., Univ. Maryland, Baltimore, Md., 1972, Academic Press, New York, 1972, pp. 589–602.
- [62] P. Grisvard, *Elliptic Problems in Nonsmooth Domains*, SIAM, 2011.
- [63] C. Canuto, A. Quarteroni, Approximation results for orthogonal polynomials in Sobolev spaces, *Math. Comput.* 38 (157) (1982) 67–86.
- [64] N.M. Wigley, On a method to subtract off a singularity at a corner for the Dirichlet or Neumann problem, *Math. Comput.* 23 (106) (1969) 395–401.
- [65] G.J. Fix, S. Gulati, G.I. Wakoff, On the use of singular functions with finite element approximations, *J. Comput. Phys.* 13 (2) (1973) 209–228.
- [66] H. Blum, M. Dobrowolski, On finite element methods for elliptic equations on domains with corners, *Computing* 28 (1) (1982) 53–63.
- [67] D. Lesnic, L. Elliott, D.B. Ingham, Treatment of singularities in time-dependent problems using the boundary element method, *Eng. Anal. Bound. Elem.* 16 (1) (1995) 65–70.
- [68] T. Strouboulis, I. Babuška, K. Copps, The design and analysis of the generalized finite element method, *Comput. Methods Appl. Mech. Eng.* 181 (1) (2000) 43–69.
- [69] L. Marin, D. Lesnic, V. Mantič, Treatment of singularities in Helmholtz-type equations using the boundary element method, *J. Sound Vib.* 278 (1) (2004) 39–62.
- [70] F.W.J. Olver, *NIST Handbook of Mathematical Functions*, Cambridge University Press, 2010.
- [71] W.H. Press, B.P. Flannery, S.A. Teukolsky, W.T. Vetterling, *Numerical Recipes in C: The Art of Scientific Programming*, 1992.
- [72] S. Brenner, Multigrid methods for the computation of singular solutions and stress intensity factors I: corner singularities, *Math. Comput. Am. Math. Soc.* 68 (226) (1999) 559–583.
- [73] B.A. Szabó, Z. Yosibash, Numerical analysis of singularities in two dimensions. Part 2: computation of generalized flux/stress intensity factors, *Int. J. Numer. Methods Eng.* 39 (3) (1996) 409–434.
- [74] G.C. Georgiou, L. Olson, Y.S. Smyrlis, A singular function boundary integral method for the Laplace equation, *Commun. Numer. Methods Eng.* 12 (2) (1996) 127–134.
- [75] C. Xenophontos, M. Elliott, G. Georgiou, A singular function boundary integral method for Laplacian problems with boundary singularities, *SIAM J. Sci. Comput.* 28 (2) (2006) 517–532.
- [76] M. Elliott, G. Georgiou, C. Xenophontos, Solving Laplacian problems with boundary singularities: a comparison of a singular function boundary integral method with the  $p/hp$  version of the finite element method, *Appl. Math. Comput.* 169 (1) (2005) 485–499.
- [77] H. Igarashi, T. Honma, A boundary element method for potential fields with corner singularities, *Appl. Math. Model.* 20 (11) (1996) 847–852.
- [78] T. Arens, S.N. Chandler-Wilde, J.A. DeSanto, On integral equation and least squares methods for scattering by diffraction gratings, *Commun. Comput. Phys.* 1 (6) (2006) 1010–1042.
- [79] E. Spence, When all else fails, integrate by parts: an overview of new and old variational formulations for linear elliptic PDEs, in: *Unified Transform Method for Boundary Value Problems: Applications and Advances*, 2014, pp. 93–159.
- [80] A.S. Fokas, J. Lenells, The Unified Transform for the modified Helmholtz equation in the exterior of a square, arXiv:1401.2502, 2014.